Development of novel applications of optical amplifiers in optical communication networks

Guo, Ning

2011

Guo, N. (2011). Development of novel applications of optical amplifiers in optical communication networks. Doctoral thesis, Nanyang Technological University, Singapore.

https://hdl.handle.net/10356/48047

https://doi.org/10.32657/10356/48047

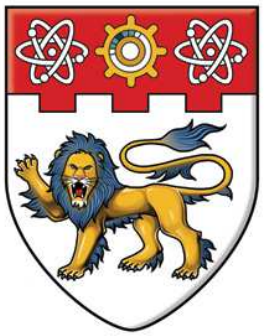

NANYANG TECHNOLOGICAL UNIVERSITY

DEVELOPMENT OF NOVEL APPLICATIONS OF OPTICAL AMPLIFIERS IN OPTICAL COMMUNICATION NETWORKS

GUO NING

SCHOOL OF ELECTICAL AND ELECTRONIC ENGINEERING

2011

.

DEVELOPMENT OF NOVEL APPLICATIONS OF OPTICAL AMPLIFIERS IN OPTICAL COMMUNICATION NETWORKS

GUO NING

GUO NING

SCHOOL OF ELECTRICAL AND ELECTRONIC ENGINEERING

A thesis submitted to the Nanyang Technological University in fulfillment of the requirement for the degree of Doctor of Philosophy

2011

ACKNOWLEDGEMENT

I would like to dedicate this page to everyone who contributes in this thesis. First of all, I would like to give thanks to Prof. Shum Ping as my project supervisors who have entrusted and given me opportunity to do this challenging project. Without your directions and encouragements, I believe that the results of our project will not be the same as the one we achieve today. By your trust in me in expressing my idea freely throughout the project, it has compelled me with strong internal motivation to do the project.

Then, I am deeply indebted to Dr Desmond Rodney Lim and Dr Vincent Wong from DSO national laboratories whose help, stimulating suggestions and encouragement helped me in all the time of research for and writing of this thesis. I would also like to express my sincere gratitude to Prof. Shien-Kuei Liaw from the National Taiwan University of Science and Technology, Taiwan, for his continuous encouragement and strong support during my PhD study.

Next I want to express my special thanks to Dr. Fu Songnian for his kind guidance, great help and fruitful discussion on my research works. Also, I would like to express my sincere thankfulness for precious discussions, suggestions and corrections from my colleagues, Mr. Zhou Junqiang in Network Technology Research Centre (NTRC). From your expertise as researcher, I have been benefited by your share of thoughts in your analytical thinking skill to solve the problems that comes along the way during the project either technically or non-technically. Finally, most of all and the greatest of all, I would like to give my deepest thank to my family.

TABLE OF CONTENTS

SUMMARY

Optical amplifier is a key component in current and future optical communication networks. It can not only provide amplification to incoming optical signals but also serve as an all-optical signal processing component. There are three categories of optical amplifiers: doped fiber amplifier (mainly erbium dope fiber amplifier (EDFA)), semiconductor optical amplifier (SOA) and Raman fiber amplifier (RFA). EDFA has larger gain, lower pump power and generally amplifies C and L band signals. While, SOA has medium gain, larger bandwidth, and higher noise figure. Most importantly, it has high nonlinearity which is very useful in all-optical signal processing. RFA requires larger pump power and has lower gain. But the bandwidth is flexible, which is determined by pump wavelength. And it has low noise figure comparing with the others.

This thesis focuses on developing novel applications of optical amplifiers in future all-optical communication networks. A detailed study on SOA gain characteristics has been done to find the origin of discrepancy between experimental measurements and simulations results given by the well-known formula. Then a modified formula which includes an additional internal loss term is proposed. It shows more accurate description on SOA gain characteristics and is proved to be able to work with different SOAs.

A novel configuration of all-optical switch utilizing nonlinear polarization rotation (NPR) in SOA is then proposed. And the switching of a data packet at 2.5 Gb/s is demonstrated experimentally with 20 dB extinction ration obtained. Furthermore, a novel configuration

of fiber loop type all-optical buffer is proposed based on the switch. Theoretical investigation has been carried out to analyze buffering results of data packets mixed with microwave signal up to 40 GHz. Thus the parameters have been optimized to obtain a buffering time of 600 ns for 40 GHz microwave signal.

Next, a hybrid C+L band pump which combines EDFA and RFA is presented. It utilizes residual pump power left from RFA for pumping of EDFA. Therefore, there is only one pumping laser diode (LD), so it is energy efficient. Moreover, an array of fiber bragg gratings (FBGs) together with dispersion compensating fiber (DCF) segments optimally compensates chromatic dispersion during transmission for all the C+L band channels. In addition, the gain fluctuation could be suppressed greatly from 6.5 dB to 0.2 dB by adjusting the reflectivities of individual FBG. Afterwards, a novel configuration of hybrid pump is proposed for application in bi-directional wavelength division multiplexing pass optical network (WDM PON). The hybrid pump is able to work bi-directionally, and it employs C-band for downstream data and L-band for upstream data. C-band signal is amplified by EDFA while L-band signal is amplified by RFA. Then, both theoretical investigations and experiments are carried out on a 50 km bi-directional WDM PON with 26 channels at 10 Gb/s data rate per channel. The required average received power for error free transmission was reduced by 3dB by dispersion compensation proposed. And gain fluctuation is suppressed from 4 dB to less than 0.5 dB by adjusting the FBG reflectivity.

Finally, conclusions are drawn and recommendations for future works are given.

Chapter 1 Introduction

1.1 Background and motivations

1.1.1 Rapid development in optical communications

In 1966, Kao & Hockham [l] published a paper in IEE Proceedings outlining the theory of dielectric single mode optical waveguides and linking them to the idea of telecommunications cable transmission using light in place of electrons. In 1970, Corning Glass Works (USA) announced the experimental achievement of fiber having an attenuation of 20dB/km [2] at the 'Trunk Telecommunications Conference' held at the IEE in London.

Optical fiber gradually becomes the transmission choice because of its large bandwidth (approximately 24 THz), low attenuation (0.2dB/km) and low transmission bit error rate(less than 10^{-9}). It serves as backbone for communication networks, while the intermediate nodes such as switches, buffers and routers still operate in electric domain. Although optical fibers are able to carry huge transmission capacity (several terabits per second), the processing speed of intermediate nodes is limited. This limitation is referred to as "electronic bottleneck". The concept of the "electronic bottleneck" was often

discussed in the late 1990's when the explosive growth of the Internet happened. The "electronic bottleneck" happens as the ability of the electronic devices has been out-stripped by the growing Internet capacity. Thus it resulted in many researchers and developers viewing all optical networks (AONs) as the solution to the "electronic bottleneck" [3, 4].

In AONs, data is transmitted in optical form throughout the whole process of transmission. That means there are no optic/electronic conversions within the network. Thus they have much higher bandwidth to be shared by the end-user. In addition, elimination of electronic/optic conversion can reduce time-delays, increase capacity, and improve flexibility of networks. Nowadays, optical transmission systems at 40 Gb/s are commercially available [5], and over 320 Gb/s technology have been demonstrated in the laboratory [6]. Additionally, various AONs test-beds and laboratory experiments have achieved an aggregate network throughput of over 1 Tb/s and higher throughputs are expected in the near future.

1.1.2 Optical amplifiers in optical communications

Optical amplifier is a key component in future AONs. It provides amplification directly to the optical signal without optic/electronic conversion. The principle of operation is similar with laser diode: stimulated emission in gain medium provides amplification to incoming

optical signals. It can be categorized into three main categories: doped fiber amplifier, semiconductor optical amplifier and Raman amplifier.

Dope fiber amplifier employs doped fiber as gain medium. A pump light triggers the doped ions to higher energy level. Then input photon stimulates the high energy ions to come down with the emission of photons which is of the same frequency, phase and direction with the input photon. As a result, the amplification is supplied by the stimulated emission. And the spontaneous emission, which is the random relaxation of high energy ions, generates noise through unwanted photons emission. The concept of doped fiber amplifier is shown in Fig. 1.1. The pump light brings the doped ions to energy level 2. Then they come down to energy level 1 through non-radiative relaxation. After that, the ions jump down from energy level 1 to ground energy level and emit photons stimulated by incoming photons.

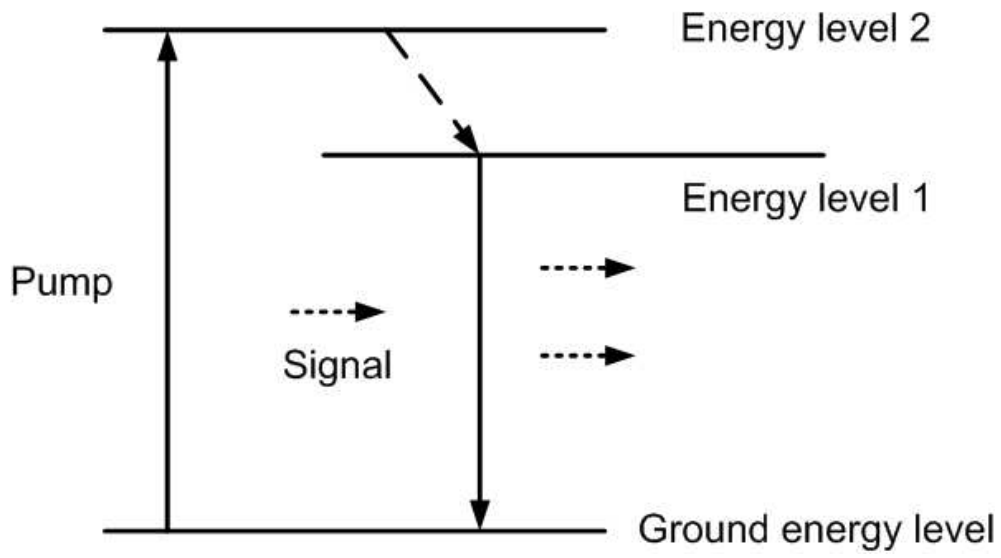

Fig. 1.1: Three level energy model for dope fiber amplifier

As the amplification is provided by the interaction of incoming light signal with the doped ions and the pump light, the bandwidth of the doped fiber amplifier is determined by the properties of the doped ions, the structure of the optical fiber, and the wavelength and power of the pump light. The erbium doped fiber amplifier (EDFA) is the most common used doped fiber amplifier in communication networks [7-8]. It was demonstrated several years after the invention of doped fiber amplifier by H. J. Shaw and Michel Digonnet at Stanford University, California, in the early 1980s. The working bandwidth of EDFA covers both the C-band (1525 nm to 1565 nm) and the L-band (1570 nm to 1610 nm), which falls in the third transmission window of the silica based optical fiber. While, the amplification of the C-band and L-band signals is usually done by two types of EDFA, one for each band. Moreover, it has two pumping bands, 980 nm and 1480 nm. 980 nm

pump light is used for low noise amplification while 1480 nm pump light is applied when high power amplification is wanted.

Semiconductor optical amplifier (SOA) is another type of optical amplifier, which employs semiconductor as gain medium. The excitation of low energy ions is done by external electric current and the process is shown in Fig. 1.2. The applied electric field separates electrons and holes into two energy levels. Then incoming light drives electrons to jump down and combine with holes accompanied by photons emission. At the same time, the spontaneous combination of electrons and holes generates unwanted photons. In addition, they can also trigger the combination of electrons and holes. Consequently, the noise accumulates, and it is therefore called amplified spontaneous emission (ASE) noise.

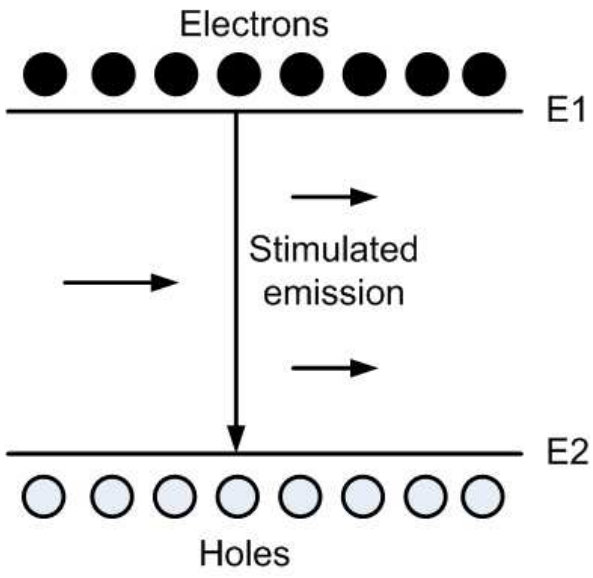

Fig. 1.2: Amplification process in SOA

Introduction

The SOA is introduced after the invention of semiconductor laser in 1960s. Zeidler and Personick start the early work on double heterostructure SOAs in 1970s [9-10]. Then AlGaAs SOA working in 830 nm range was demonstrated in early 1980s [11-12]. In later 1980s, lnP/lnGaAsP SOAs working in 1300 nm and 1550 nm range was invented [13]. Later on, true travelling wave SOA is realized with the help of anti-reflection coating technology in 1988 [14]. And the polarization sensitivity is reduced by using more symmetrical waveguide [15].

Compared with EDFA, SOA has lower gain and higher noise, but it also has advantages of compact size, easy integration, etc. Moreover, the high nonlinearity of SOA makes it not only an amplifier to incoming signal but also a key component in all-optical signal processing.

Raman amplifier amplifies signal through Raman amplification. Raman amplification originates from the interaction between lightwaves and vibrational modes of silica molecules [16-17]. It can transfer energy from shorter wavelength to longer wavelength. Aoki et al demonstrated optical data transmission using Raman amplification [18]. And Mollenauer et al. utilized a fiber Raman amplifier to carry out optical soliton transmission [19].

There are two types of Raman amplifiers: distributed and lumped. Distributed Raman amplifier utilizes the whole transmission line as gain medium and lumped Raman amplifier employs a dedicated short fiber segment to provide amplification. Compared

with SOA and EDFA, Raman amplifier has flexible bandwidth as it is determined by the pump wavelength. It also has low noise figure and fast response time. However, Raman amplifier requires high pump power and has low gain.

In this thesis, we are going to investigate novel applications of various optical amplifiers not only in current communication networks, but also in future all-optical communication networks.

1.1.3 All-optical buffer

To realize all-optical network various components are needed, while all-optical buffer plays an important part. Buffer is a key part of the router and it solves the packets contention problem by temporarily storing/reading out packets overlap in time domain according to their priorities. All-optical buffer is a type of buffer which operates purely in optical domain. The conceptual schematic of all-optical buffer is shown below:

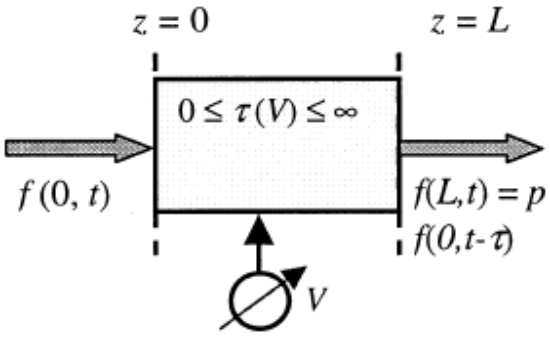

Fig. 1.3: Schematic of Optical Buffer

The output data stream f(L,t) is essentially a copy of the input data f(0,t); it is equal to the multiplication of a proportionality constant p with a time delay that is variable controlled by an external source V.

The buffering time can be expressed as follows:

$$\tau = \frac{L}{V_g} \tag{1.1}$$

According to the equation above, there are two ways to determine the buffering time τ. One is increasing the path length L, which corresponds to fiber delay line type optical buffer. The other is decreasing the velocity V_g, which corresponds to slow light type optical buffer. At first, the only practical optical buffer is the fiber delay line type which consists of space-consuming fiber loops or various folded free space designs. Lately, however, there been a remarkable progress in the development of slow light type which alters group velocity of the light.

1.1.3.1 Fiber Delay Line type Optical Buffer

The basic design of fiber delay line optical buffer consists of an optical switch connected with a fiber loop, as shown in Fig. 1.4.

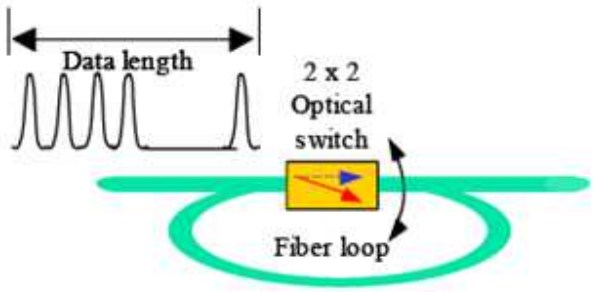

Fig. 1.4: Basic design of fiber delay line type optical buffer

In 1996, R. Langenhorst. et al. presented a detailed theoretical and experimental investigation on fiber loop optical buffer using semiconductor optical amplifiers (SOAs) as switches [20]. The configuration of the optical buffer is shown in Fig. 1.5. In the configuration, S stands for SOA. So there are four SOAs in the scheme: Sin, Sout , Sc, and Sp. Sout provides connection between buffer and transmission line via 3dB fiber couplers. Sc compensates loss inside the loop and prevents ring laser operation by periodically electrical gating of the loop. Sp enables a passage of data without storage in loop.

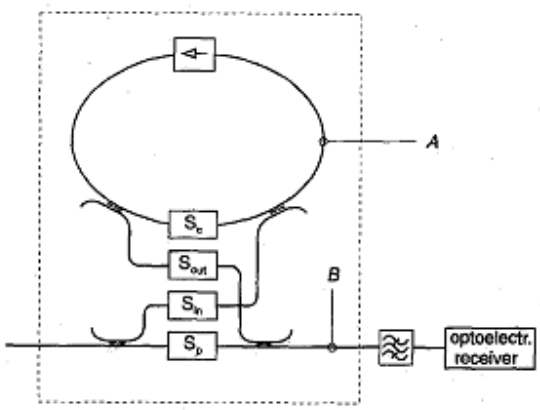

Fig. 1.5: Configuration of a fiber loop type optical buffer

The experimental results show that error free storage of a 622Mb/s, 312bits long data packets for 40 circulations (20μs) can be realized. But this configuration requires four SOAs, which is not economical. In addition, the SOAs are controlled electrically as switches. Thus this configuration is not the real "all optical buffer".

In 1999, Xiaobin Hong et al. proposed an erasable fiber loop optical buffer [21], as shown in Fig.1.6. The SOA (SLA in the diagram) serves as a nonlinear element as well as an optical amplifier. The control pulse introduced by wavelength division multiplexer (WDM) induces different phase variation for the clockwise and counters clockwise signal. After recombination at coupler 2, the signal appears at port B, and then travels inside the loop. In case of no control pulse injection, the signal appears at port A and then is terminated by the isolator. In this configuration, the control pulse remains in the loop after interaction with input signal in SOA. It is not guided out of the loop, and this could cause channel

cross talk problems. Moreover, this configuration cannot handle the packets which are not intent for buffering.

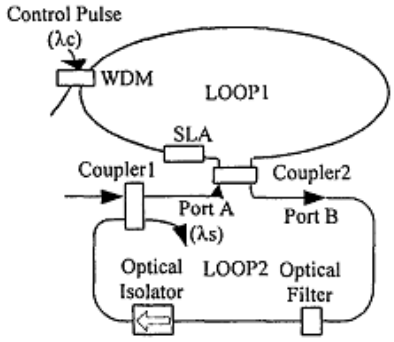

Fig. 1.6: Schematic diagram of a fiber loop type optical buffer

In 2004, A.M. Liu et al. found a dual loop optical buffer based on a collinear fiber coupler [22]. The experimental setup is shown below:

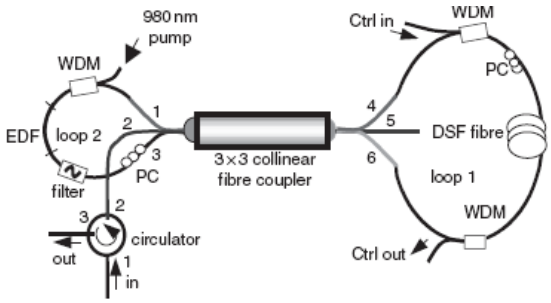

Fig. 1.7: Experimental setup of dual loop optical buffer

The dispersion shifted fiber (DSF) introduces unequal phase change in clockwise and counter clockwise directions in case of control signal injection. When recombining at coupler, the signal emerges at port 1 and 3 of coupler. Thus the signal is trapped inside the

loop. Storage of 16 bits data packet at 2.5Gb/s for 1.568ms has been demonstrated through experiment. However, the required optical power of control signal is very high in order to introduce sufficient phase change within 3km DSF. And the required fiber length is very long, so that the walking-off effect cannot be ignored.

In 2006, Songnian Fu et al. presented detailed theoretical and experimental analysis of a semiconductor optical amplifier (SOA) based dual loop optical buffer [23]. The schematic is shown in Fig. 1.8.

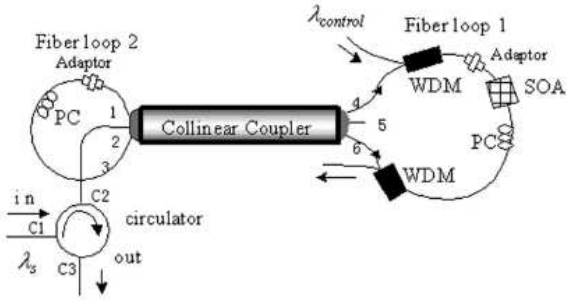

Fig. 1.8: Schematic of SOA based dual loop optical buffer

The nonlinear element DSF has been replaced by SOA in this setup comparing with the previous setup. And the result of 16 bit 2.5Gb/s data packet storage for 1.6μs has been achieved.

Besides fiber loop optical buffer, other type of buffer has also been proposed. For example, Chin Hui Chen et al. proposed a fiber brag grating (FBG) based optical buffer in 2005 [24]. The experimental set up is shown below:

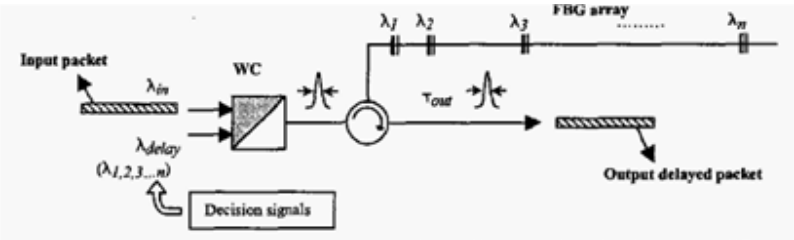

Fig. 1.9: Schematic of FBG based optical buffer

The input packet goes through wavelength conversion (WC) first. The resultant wavelength decides from which point of the FBG array the signal reflects back. Thus a process of wavelength conversion is required for each packet, which is time consuming. Also, for this type of optical buffer, the buffering time is limited by the fiber length. Thus it is bulky in terms of size.

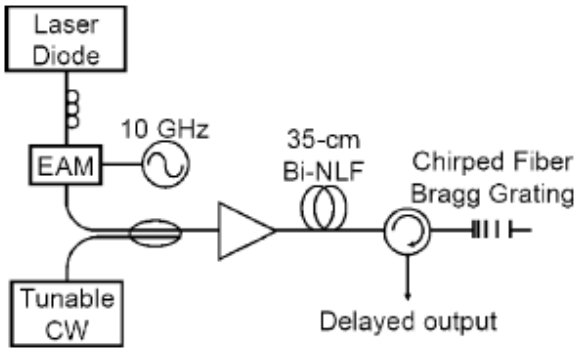

Fig. 1.10: Schematic of CFBG and Bi-NLF based optical buffer

In 2008, Mable P. M. et al. presented a new scheme of optical buffer based on FBG [25]. The experimental set up is presented in Fig. 1.10. It utilizes four wave mixing (FWM) wavelength conversion in a 35cm highly nonlinear bismuth-oxide fiber (Bi-NLF). The Bi-

NLF serves as the wavelength converter in the previous scheme reported. A delay up to 840 ps has been demonstrated experimentally. This scheme also has the problem of bulky size as the buffering time depends on the CFBG length.

Park H. et al. proposed a scheme of optical buffer using silicon waveguide delay lines and a silicon evanescent gate matrix switch in 2008 [26]. The result of an error free operation at 40 Gb/s data rate with a packet delay of 1.1 ns is demonstrated. But the problem of polarization of the signal is not considered and the buffering time is fixed. More importantly, the control signal is electronic, which means this is not a real all-optical buffer.

In 2011Berrettini G. et al. introduced a variable all-optical buffer based on SOA [27]. It utilized the cross gain modulation (XGM) in SOA to realize the buffering effect. The power level of the control signal decides whether the packet should be read out or writes in. And a buffering result of 50 μs is obtained for a 10 Gb/s packet. But this configuration employs two SOA, which is expensive. And the signal travels through two SOA, which could also introduce more ASE noise.

To make a conclusion, the fiber loop optical buffer is compact in terms of size comparing with other types of optical buffer. It also provides a longer buffering time and it is easy to implement. Furthermore, SOA is usually used as a switching nonlinear element because of its fast recovery time, small footprint and potential integration with other devices. The

buffering time is easy to adjust by increasing the number of circulations. Moreover, the polarization of the signal has a large impact on the storage results.

1.1.3.2 Slow Light Optical Buffer

Slow light technology decreases group velocity of light inside a waveguide or device by various means. The group velocity of light could be expressed as follows:

$$v_g = \frac{\partial \omega}{\partial k} = \frac{c - \omega \dfrac{\partial n(k,\omega)}{\partial k}}{n(k,\omega) + \omega \dfrac{\partial n(k,\omega)}{\partial \omega}} \tag{1.2}$$

There is an important parameter slow down factor S which is defined as:

$$S = \frac{c}{v_g} = \frac{n + \omega \dfrac{\partial n}{\partial \omega}}{1 - \dfrac{\omega}{c}\dfrac{\partial n}{\partial k}} \tag{1.3}$$

The slowdown factor increases as the group velocity decreases. Seen from equation (1.3), there are two ways to increase the S. One way is to introduce large waveguide dispersion $\frac{\partial n}{\partial k}$. The other way is to introduce a large and positive material dispersion $\frac{\partial n}{\partial \omega}$.

Based on different methods used, slow light could be categorized into several classes:

1. Waveguide dispersion based slow light.
2. Electromagnetically introduced transparency (EIT) based slow light.
3. Stimulated Brillouin Scattering (SBS) based slow light.
4. Other type of slow light.

In 2000, Jacob. B. Khurgin reported a slow light method using the waveguide dispersion in Moiré fiber grating [28]. Experiment showed that the reduction of speed of light could be S = 100 to 1000.

In 2001, G. Lenz et al. performed both theoretical and experimental investigation on slow light resulted from waveguide dispersion in optical filters [29]. Delay up to 150ps has been achieved.

Both EIT and SBS based slow light are to introduce a large positive $\frac{\partial n}{\partial \omega}$. EIT introduces a control light which is near resonance with the transition |3> to |2>, which is shown in Fig. 1.11. In such a case, the two possible transitions in which light could be absorbed (|1> to |2> and |3> to |2>) will interact and cancel each other. Thus it results in a small transmission window, inside which the material could be thought as transparent. However, the narrow transparence resonance is accompanied by a larger variation of refractive index with respect to frequency as shown in Fig. 1.12.

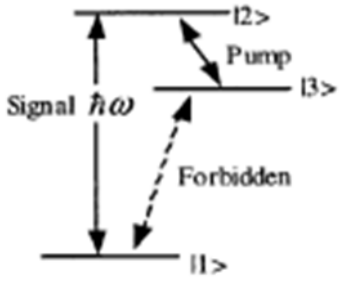

Fig.1.11: Prototype atomic system for EIT

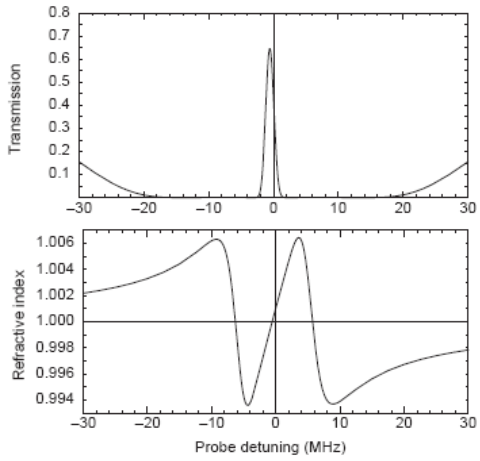

Fig. 1.12: Spectrum for transmission and refractive index change

The EIT based slow light achievements are summarized in the tables below:

Table 1.1: EIT based slow light achievements

	Medium	Experimental temperature	Velocity of light
L. V. Hau, Nature, 397,594, 1999	Na vapor	Ultracold (<100 nK)	17m/s
D. F. Philips, Phys. Rev. Lett., 86, 783, 2001	Rb vapor	70-90°C	1 km/s

A. V. Turukhin, et al., Phys. Rev. Lett., 88, 023602, 2002	Pr doped Y2SiO5 crystal	5 K	45m/s
P. C. Ku, et al., Electro. Lett., 38, 1581, 2002	Semiconductor quantum dots structure	Room temperature	9600m/s
E. Baldit, Phys. Rev. Lett., 95, 143601, 2005	Erbium doped crystal	1.5 K	2.7m/s
Bashkansky M., et al., Phys. Rev. A., 72, 033819, 2005	Rb vapor	65°C	7.5 km/s
Zhang J., et al., Optics lett. 33, 46, 2008	Rb vapor	cold	4.8 km/s

In SBS system, probe signal at frequency f_{probe} counter-propagating with pump signal at frequency f_{pump} will be amplified at $f_{pump} - \nu_B$ (ν_B is the Brillouin frequency) while suppressed at $f_{pump} + \nu_B$. The gain and refractive index change versus frequency is shown in Fig. 1.13. The strong coupling between pump and probe signal via an acoustic wave (corresponding to ν_B) results in large refractive index change versus frequency at probe frequency.

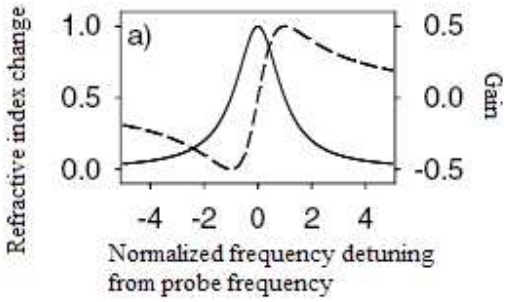

Fig. 1.13: Gain (dash line) and refractive index (solid line) change versus normalized frequency

The SBS based slow light achievements are listed in Table 1.2:

Table 1.2: SBS based slow light achievements

	Fiber type	Power of pump	Gain	Max. delay	bandwidth
Kwang Y. S., Optical Express, 13, 82, 2005	SMF 11.8 km	Tens of mW	30dB	30ns	35MHz
Yoshitomo, Phys. Rev. Lett., 94, 153902, 2005	DSF 0.5 km	250mW	29dB	25ns	30MHz
Herraze, Optics Express, 14, 1395	DSF 6.7 km	30mW	30dB	2.7ns	325MHz
Zhu Z., Optical Fiber Communication Conference 2005	HNLF 2 km	580mW	14dB	47ps	12.6GHz
Jauregui C., Optical Fiber Communication Conference 2006	Bi-HNLF 2m	410mW	29dB	46ns	40MHz
Yoshitomo O., Conference on Laser & Electro-optics 2005	SMF 500m	10nW	20dB	16ns	70.3MHz
Zhu Z., Optics Express, 14, 7238, 2006	HNLF 2 km	13dBm	12.3dB	9ns	150MHz
Yi L., et al., Phton. Tech. Lett., 19, 619, 2007	SMF 12.5 km	23dBm	12dB	520ps	1.25GHz
Yi L., et al., Optics Express, 15, 16972, 2007	Ture wave (TW) fiber 20 km	22dBm	10.8dB	81.5ps	10GHz

In [30], Jay E. Sharping et al. proposed a slow light method employing a Raman fiber amplifier. The experiment demonstrates delay of 430fs pulses by 85% of a pulse width. The bandwidth of the system could accommodate that of pulse width less than 1ps.

Zhangyuan Chen et al. reported a method of slow light via four wave mixing (FWM) in SOA [31]. A delay of 900 ps is realized and the bandwidth is 500 MHz.

In 2005 Daisuke Mori and Toshihiko Baba investigated slow light by chirped photonic crystal coupled waveguide. The slowdown factor could be 450 for a signal bandwidth of 40 GHz in the experiment [32].

Recently, Horak P. et al. presented a continuously tunable optical buffer comprised two coupled silicon waveguides [33]. A delay bit rate product of 40 is achieved.

After comparing the fiber delay line optical buffer with the slow light optical buffer, we found that the fiber delay line optical buffer could provide larger delay and larger bandwidth. The former could provide time delay up to ms while the latter provides only ps. Also the slow light usually requires strict experimental environment, for example, low temperature, high optical power, etc. Consequently, the former is easier to implement. Thus our research will mainly focus on fiber delay line type optical buffer. Moreover, SOA plays an important role in most of optical buffer configuration because of its compactness, small footprint, high nonlinearity and fast response time. As a result, my research will also investigate the fiber delay line type optical buffer utilizing nonlinearity of SOA.

1.1.4 Wavelength division multiplexing passive optical network (WDM PON)

WDM PON is another promising technology to realize future all-optical network (AON). Today's dense WDM (DWDM) system is capable of working with 50 GHz or even 25 GHz channel spacing for up to 160 channels [34]. It becomes a promising technology with the development in scalability, capacity and reliability [35].

WDM passive optical networks (PONs) employ WDM technology inside PONs, which was originally developed in the 1980s [36]. The basic PON structure is shown in Fig. 1.14. Initially, it was designed for the sharing of fiber infrastructure for narrow band communications. Technologies like Broadband PON (BPON), Ethernet PON (EPON) and Gigabyte PON (GPON) [37] share the same idea of sharing the fiber by time division multiplexing (TDM) while WDM offers alternative ways of sharing the optical medium. The advantages in terms of capacity, service transparency and reliability make WDM a vital technique in PONs.

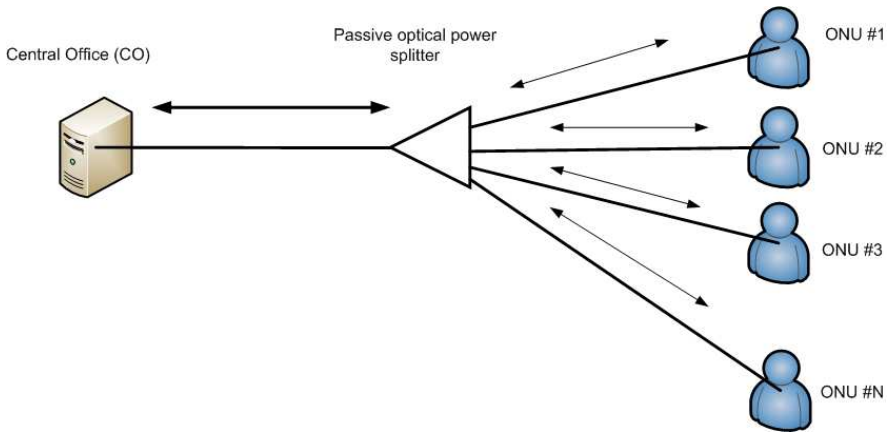

Fig. 1.14: Basic PON structure

WDM PON utilizes the WDM techniques to offer sharing of capacity of PON between different users. Recently it receives considerable interest because of its advantages of low latency, large capacity and service transparency. The common WDM PON structure is shown in Fig. 1.15.

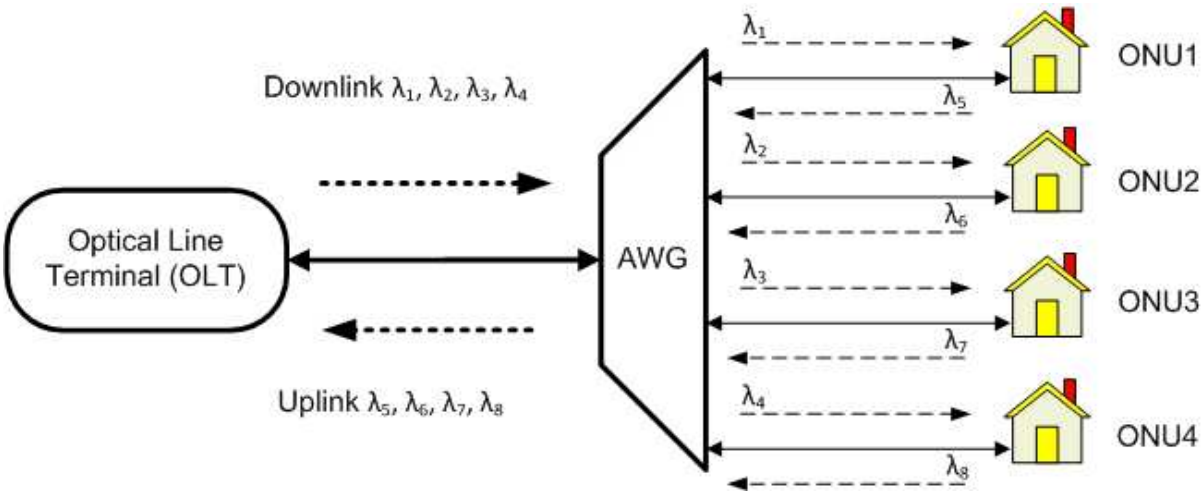

Fig.1.15: WDM PON structure

Optical line terminal (OLT) is the central office that sends out all the data through downlink with different wavelengths targeted at different users. Optical network unit (ONU) at the user side receives or sends out the respective data at designated wavelengths. An array wave guide grating (AWG) is employed to separate downlink data into different wavelengths for different ONU and combine uplink data at different wavelength from different ONU. At the ONU side a receiver processes the downlink data sent out from OLT while a reflective modulator is required for the uplink data. In this configuration, there is no active component except OLT. And that is why it is called “passive optical network”.

The advantages of wavelength division multiplexing (WDM) passive optical network (PON) such as easy upgradability and excellent security make it a promising candidate for future AON. Moreover, the rapid growing data traffic in WDM PON drives the extensive study of wideband amplifiers as they are drawing more and more attention. Conventional erbium-doped fiber amplifiers (EDFAs) operating in the C-band wavelength-division-multiplexing (WDM) system is quite mature nowadays. However, because the entire C band is fully utilized, the demands of wider bandwidth for optical amplification are studied extensively in WDM systems. For the L-band amplification, Raman fiber amplifier (RFA) is known to have a lower noise figure (NF) than that of the L-band EDFA [38]. Consequently, a hybrid amplifier is highly promising for multi-terabit dense WDM

(DWDM) systems. A hybrid Raman/Erbium-doped fiber amplifier was designed for maximizing the span length and/or minimizing the impairments of fiber nonlinearities. It was also used to enlarge the EDFA gain-bandwidth [39]. Recently, plenty of works have been done on WDM PON. But the performance of the network is greatly limited by fiber loss which limits the reach of network within 25 km [40-43]. To solve this problem, remote pumping is proposed to extend the network span. Most of remote pumping amplifiers serve as preamplifiers to provide amplification thus extends the reach of the network. One issue is that the working range of conventional erbium-doped fiber amplifier (EDFA) only covers C band. Although EDFA is able to work in L band, additional pumping source and extra gain fiber is needed. To utilize L band in WDM PON and thus increase the capacity of the network, Raman fiber amplifier (RFA) with lower noise figure (NF) is a more attractive solution for remote pumping. Another factor which degrades the performance of the WDM PON is the chromatic dispersion in the lightwave transmission. Consequently, dispersion compensating fiber (DCF) is usually implemented to provide either pre- or post-transmission compensation of fiber dispersion.

In previous work, a wide-band and gain-flattened hybrid RFA/EDFA using several pump lasers was demonstrated in [44]. However, the employment of multi-pump lasers is unavoidable for such hybrid EDFA/RFA configuration, which increasing the cost and the system complexity. In [45], a C-band RFA was employed to control and flatten the entire gain profile of an in-line EDFA. However, the operating spectral range was restricted to the C band. The device proposed in [46] was a dispersion-compensating hybrid amplifier

with two pump lasers at wavelengths of 1545 and 1565 nm. Recently, Nicholson et al. proposed the usage of fiber Bragg gratings (FBGs) to reflect the residual pump power back into the DCF as a secondary pump source. They experimentally demonstrated the enhancement of the whole Raman gain profile [47]. Another theoretical study was carried on the cascaded EDFA/RFA scheme, which is pumped bi-directionally using a 1495 nm pump laser [48]. However, the gain-flattening and dispersion management for C+L band channels in that hybrid amplifier scheme have not yet been achieved simultaneously. In [49], a 1411 nm pump laser was used to convert a 1490 nm Raman pump for serial type of C/L EDFA/RFA. However, the loop mirror introduced a 3 dB extra loss, which is a drawback.

In [50], a gain equalized C+L hybrid amplifier by properly adjusting the pump power ratio is demonstrated. However, the residual dispersion is a problem and precise gain equalization was not yet achieved. In [51], a serial type hybrid C+L band scheme was presented. A bridge-type, hybrid C+L band EDFA/RFA using a single pump laser diode (LD) was first proposed and investigated. Optimum dispersion compensation and power equalization for all C+L band channels are simultaneously realized. This scheme could simultaneously flatten the gain profile and manage the gain module dispersion.

In [52], another scheme for both dispersion compensation and gain equalization was investigated, but it is limited to C band Raman amplification.

In this thesis, we aim at proposing a novel schematic of amplifier for WDM PON. It should have the capability of amplifying both C and L band signals. It should also provide optimized dispersion compensation and gain equalization.

1.2 Objectives

The main objective of this thesis is to investigate the applications of optical amplifiers in optical communications. In order to utilize the SOA to construct optical network components, gain characteristics of SOA are to be detailed studied. The proposed formula should accurately describe the saturation effect of the gain under large injection power. Furthermore, new types of all-optical signal processing components are going to be proposed. By utilizing nonlinear polarization rotation (NPR) in SOA, a new configuration of all-optical switch is to be proposed. Experimental works should be done to prove the feasibility of the all-optical switch. Furthermore, a new configuration of loop type all-optical buffer is going to be presented based on the all-optical switch proposed. Theoretical investigations should be done to analyze the optical signal storage. Also, operation parameters should be optimized. Another objective is to develop a new hybrid pump for wavelength division multiplexing (WDM) passive optical networks (PONs) using erbium dope fiber amplifier (EDFA) and Raman fiber amplifier (RFA). Conventional EDFA covers downlink while the uplink is amplified by lumped RFA which

has a lower noise figure than L-band EDFA. First, a unidirectional hybrid pump with single pump laser diode will be introduced. The hybrid pump should also suppress gain variation and compensate chromatic dispersion along the link. Next, a bidirectional hybrid pump is going to be proposed. The pumping laser diode wavelength is going to be shifted to cover the whole L-band.

1.3 Outline of the thesis

After introduction in chapter 1, chapter 2 will look into the gain characteristics of SOA. The existing formula describing the gain characteristics of SOA is investigated and obvious discrepancy from experimental measurements is found. A term related to internal loss inside active region of SOA is introduced. Thus a new formula is proposed. By comparing the simulation results obtained from the proposed formula and the experimental measurements, the accuracy of the proposed formula is proved to be much better than the existing formula. Experimental measurements performed on another SOA from a different company also show the feasibility of this formula to different types of SOA.

In chapter 3, all-optical network components utilizing nonlinearity from SOA is proposed and investigated. Nonlinear polarization rotation (NPR) in SOA is employed to construct an all-optical switch first. A linear polarization state is maintained during the process of NPR. A 2.5 Gb/s data packet containing 500 bytes pseudo random binary sequence (PRBS) data is switch successfully from one output port to another. And the eye diagrams obtained prove the workability of the proposed all-optical switch. Next, a novel scheme of all-optical buffer based on the all-optical switch is proposed. It is constructed using the switch proposed together with a segment of polarization maintaining fiber (PMF). Theoretical investigations are performed to analyze the storage of microwave signal storage up to 40 GHz. And operation parameters of the buffer are optimized to get the best results.

A hybrid C+L band pump combining EDFA and RFA is proposed in chapter 4. EDFA is used to provide C-band signal amplification and the L-band signal is amplified by a lumped RFA. A unidirectional hybrid pump is introduced first. In the proposed configuration, single pumping LD is used. In addition, the hybrid pump is able to suppress the gain variation and compensate the chromatic dispersion at the same time. A carefully designed dispersion shift fiber (DCF) array together with a group of fiber bragg gratings (FBGs) do the job. Lengths of DCF are calculated and reflectivities of FBGs are optimized to get the best results. Theoretical investigations prove the hybrid pump is able to work with negligible intra-band cross talk and low noise figure. Moreover, the residual pump reuse improves the efficiency of the system. Then, a hybrid pump which is able to

work bi-directionally is proposed. The pump LD wavelength is also shifted to longer wavelength in order to cover the whole L-band. Theoretical study shows that the hybrid pump is able to work in 26 channels 50 km WDM PON with channel data rate at 10 Gb/s.

Chapter 5 summarizes the main achievements and draws the conclusions of the thesis. Discussions and recommendations of possible future works are presented.

1.4 Original contributions

The original contributions of this thesis as listed as follows:

- Proposal and experimental investigation of a formula describing the gain characteristics of SOA with greatly improved accuracy comparing with the existing formula. (chapter 2)
- Design and demonstration of a new configuration of all-optical switch based on NPR in SOA. (chapter 3)
- Proposal and theoretical investigation of a new type of all-optical buffer based on NPR in SOA. (chapter 3)

- Proposal and theoretical investigation of a novel unidirectional bridge type hybrid EDFA/RFA pump with the ability of achieving gain equalization and chromatic dispersion compensation at the same time. (chapter 4)

- Proposal and investigation of a novel bidirectional hybrid EDFA/RFA pump for WDM PON application. Experiments are carried out to prove the feasibility of the hybrid pump. The hybrid pump is able to cover the whole C+L band. (chapter 4)

Chapter 2 Gain Characteristics of Semiconductor Optical Amplifier

2.1 Introduction

The advancement of semiconductor fabrication techniques and device design make semiconductor optical amplifier (SOA) a great component for all optical communication networks. It does not only provide amplification to optical signal, but also play an important role in all-optical signal processing. The advantages of SOA such as small footprint, low power consumption, and potential optical integration have drawn considerable attention for all-optical signal processing during the past years [53]. When SOA works in linear the input signal is amplified linearly by stimulated emission. In that case, it serves as an amplifier. While, if the input signal power increases to the extent that the carrier depletion occurs in SOA active region, gain saturation eventually occur. It is a serious problem in multi-channel systems as it leads to inter-channel crosstalk [54]. Meanwhile SOA working in saturation region exhibits several nonlinear behaviors, such as cross phase modulation (XPM), cross gain modulation (XGM), and four wave mixing

(FWM). All have been utilized to demonstrate function devices for all-optical signal processing application [55] successfully. Therefore, the gain saturation characteristics of SOA have drawn a lot of attention [56-57]. Another important characteristic of SOA is high nonlinearity, which plays an important part in all-optical signal processing. We could utilize its nonlinearities to construct network component other than just use it as amplifier. In the next chapter, we will investigate the application of SOA in all-optical buffer. Optical buffer is one of the most important components in all-optical networks (AONs). It has the ability of storing data packets for controllable period of time to avoid packet contention. There are various types of all-optical buffer reported. And we will give a literature review on current all-optical buffer in the following section.

This chapter explores the gain characteristics of SOA in detail. Section 2 gives a literature review of existing theory on SOA gain characteristics and the current achievements in all-optical buffer. And the next chapter will present our proposal of all-optical buffer based on nonlinearities in SOA. In section 3, we find that the theoretical results derived from the well-known SOA gain formula [58] deviate greatly from the experimental measurements. In section 4, we investigate the effect of absorption loss on the gain characteristic of SOA and find that the absorption loss ignored previously becomes significant when the SOA is operated at saturation region. Then, a modification to the common-use formula is proposed and verified against the experimental measurements to show that the proposed theoretical formula can be applied to evaluate the SOA gain characteristics in practical. Finally, conclusions are given in section 5.

2.2 Literature Review

Semiconductor optical amplifier is key component in communication networks. The structure is similar to a laser diode except the facets have anti-reflection design [59]. The incoming signal is amplified by stimulated emission (combinations of electrons and holes). The common structure of SOA is shown in Fig. 2.1.

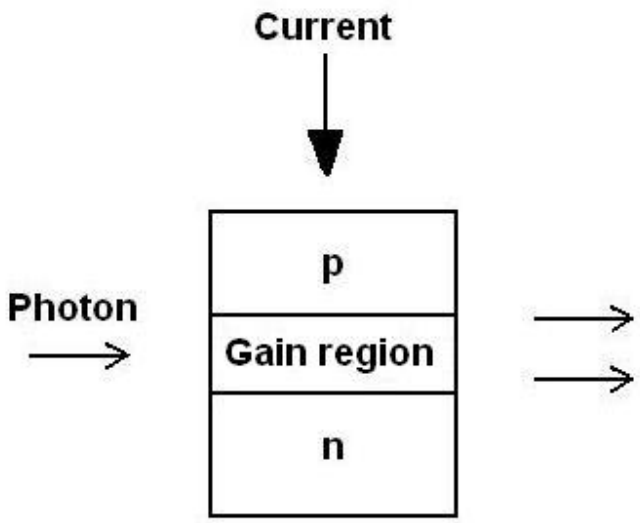

Fig. 2.1: Structure of SOA

The holes in p cladding and electrons in n cladding are driven to the gain region by biasing current. Then, they recombine in the gain region either through stimulated emission or spontaneous emission. The stimulated emission induced by the incoming photons provides the useful amplification while the spontaneous emission introduces

unwanted noise. The gain region has a lower band-gap and a higher refraction index that the cladding layer. As a result, the refractive index difference produces a wave-guide for the signal light. Early SOA is made from AlGaAs and works in 830 nm range [60-61]. Later, lnP/lnGaAs is introduced in late 1980's to construct SOA. And the operating wavelength shifts to 1.3 μm and 1.55 μm range, which is the working wavelength range of optical communication network today [62].

Nowadays, SOA is able to provide gain up to 30 dB according to the datasheets provided. However, these gain figures given in commercial SOA data sheet is obtained at -20 dBm input signal power, and it is called the small signal gain.

The SOA gain depends on wavelength of incident signals. The following formula describes the gain coefficient for SOA (gain per unit length):

$$g(\omega) = \frac{g_0}{1 + (\omega - \omega_0)^2 T_2^2 + P / P_s} \tag{2.1}$$

where g_0 is the maximum gain, ω is frequency of the incident signal, ω_0 is the atomic transition frequency and P is the incident signal power, P_s is the saturation power of the gain medium and T_2 is the dipole relaxation time, and the typical value for semiconductor is 0.1 ps.

For small signal (low input power) $P/P_s << 1$, the above equation could be simplified to:

$$g(\omega) = \frac{g_0}{1 + (\omega - \omega_0)^2 T_2^2} \tag{2.2}$$

Obviously, the gain maximizes at ω_0 and the gain profile is Lorentzian. The gain bandwidth is defined as the full width half maximum (FWHM) of the gain spectrum g(ω) and is given by:

$$\Delta\nu_g = \frac{\Delta\omega_g}{2\pi} = \frac{1}{\pi T_2} \tag{2.3}$$

For a typical semiconductor, T_2 is approximately 0.1 ps. Thus the typical value of $\Delta\nu_g$ is approximately 3 THz. This value is the bandwidth of the gain spectrum. When we come to component level, the parameter we cares is the gain bandwidth $\Delta\nu_a$, which could be related to $\Delta\nu_g$ by the following equation:

$$\Delta\nu_a = \Delta\nu_g \left(\frac{\ln 2}{g_0 L - \ln 2}\right) \tag{2.4}$$

where L is the amplifier medium length.

The gain will saturates at a point if the input signal power keeps on increasing. Afterwards, the gain will decrease with increasing input signal power. The gain saturation concept is demonstrated in Fig. 2.2.

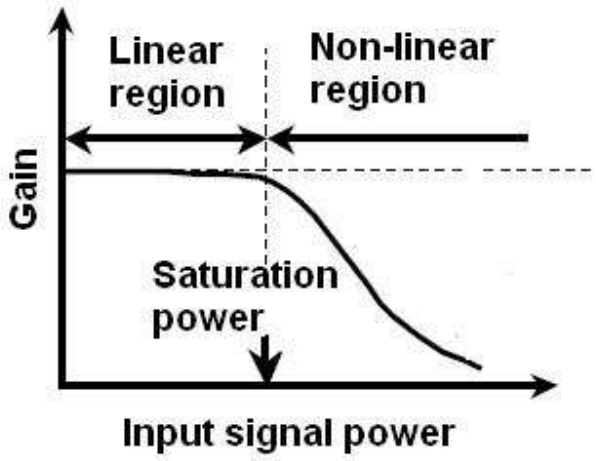

Fig. 2.2: Gain saturation concept

The gain saturation originates from the depletion of electron-hole pairs together with other losses incurred by the propagating signal travelling inside SOA gain region. And it draws great attention as nonlinearities of SOA (such as XGM, XPM and FWM) found a lot of applications in all-optical signal processing [63-65].

We define the gain as the ratio between output power and input power:

$$G = \frac{P_{out}}{P_{in}} \tag{2.5}$$

where P_{out} and P_{in} is related by the amplifier equation:

$$\frac{dP}{dz} = gP \tag{2.6}$$

where P(z) is the power at a distance z from the input end.

For simplicity, we take the case when $\omega=\omega_0$. By combining equation 2.1 with equation 2.6, we get:

$$\frac{dP}{dz} = \frac{g_0 P}{1 + P / P_s} \tag{2.7}$$

using boundry condition P(0) = P_{in} and P(L)=P_{out} we get the well-known formula describing the gain characteristics[58]:

$$P_{out} = P_{in} G_0 \exp[-\frac{(G-1)P_{in}}{P_s}] \tag{2.8}$$

where P_{in} is SOA input power and P_{out} is SOA output power. The amplifier gain G is the ratio of the output and input signal power. $G_0 = \exp(g_0 L)$ is the small-signal gain of SOA, g_0 is small signal gain coefficient, and L is the length of active region. P_s is known as the saturation power of the gain medium. However, P_s cannot be obtained from experiments directly. It is related to the saturated output power P_{sout}, which can be given by $P_{sout} = \frac{G_0 \ln 2}{G_0 - 2} P_s$. A rough calculation based on the formula is present in Fig. 2.3.

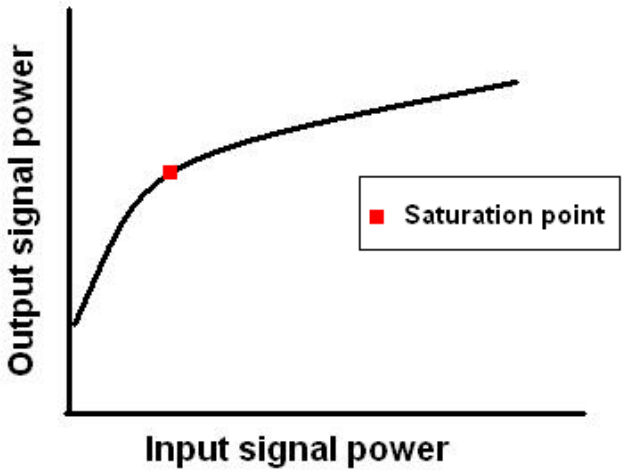

Fig. 2.3: Calculation based on equation 2.1

The gain decrease with increasing input signal power, but the gain saturation phenomenon is not obvious, as the output signal power cannot converge to a particular value eventually. Saturation point is defined as the point where the gain of SOA decreases from its small signal gain by 3 dB.

2.3 SOA Gain Characteristics Measurement

We need to set up an experiment to measure the gain characteristics of an SOA in order to verify the validity of equation 2.8.

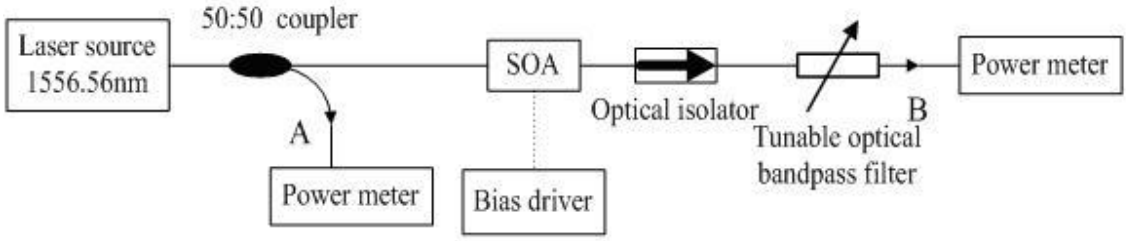

Fig. 2.4: Experimental setup for measuring gain characteristics of SOA

The experimental setup to measure the SOA gain characteristic is shown in Fig. 2.4. The dashed line indicates the electrical path, while the solid lines symbolize the optical paths. An SOA from Kamelian Corporation is used in this experiment. Considering the coupling loss at each end of SOA, a 6 dB margin has been added to the given small-signal gain value. This coupling loss includes the coupling loss between SOA active region and tapered fiber, and the tapered fiber splicing loss. Since SOA has irregular active region, there will be coupling loss from active region to tapered fiber. And we splice two connectors to both tapered fiber, so fiber splicing loss applies in this case. Thus the final value is $G_0 = 792$ when the SOA is biased at 200mA and thermally stabilized at 20°C. The continue wave (CW) optical signal is generated by a 1556.56nm distributed feedback (DFB) laser module. Then, it is equally separated into two parts with a 3dB coupler. One part is used to monitor the input power at point A in Fig. 2.4. The other part is injected into the SOA. At the output of SOA, one optical isolator is used to ensure unidirectional propagation in the experimental setup and suppress undesired reflections. The removal of Amplified Spontaneous Emission (ASE) noise is performed by a 1-nm tunable optical

band-pass filter after calibration with DFB operation wavelength. Finally, we take measurement at point B in Fig. 2.4 to obtain the output power after amplification. The SOA biasing current can be easily adjusted by the driver.

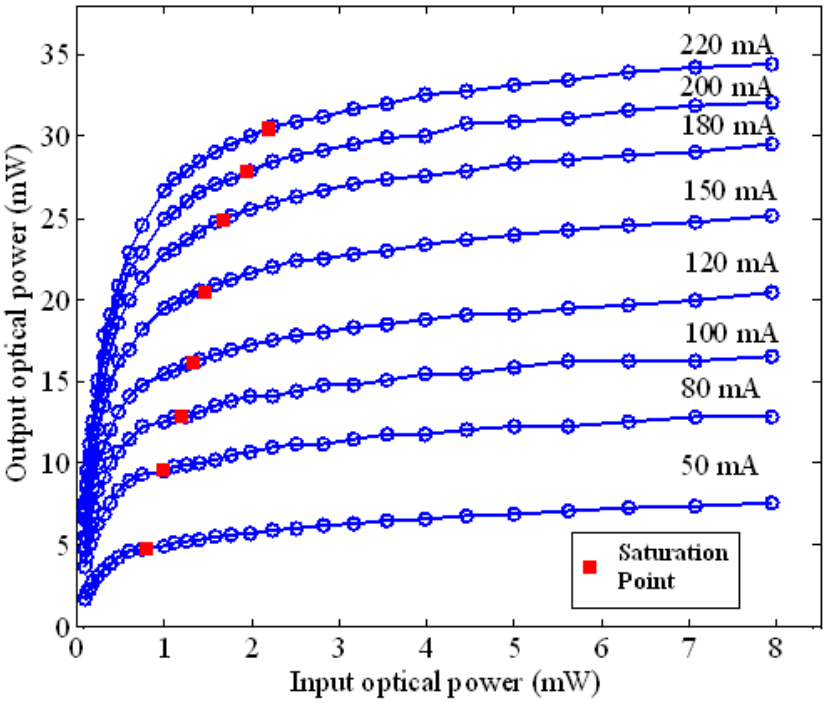

Fig. 2.5: Experimental measurements of gain characteristics of SOA

The measured gain characteristic with respect to the input optical power under different biasing currents is shown in Fig. 2.5. As we can observe, the gain eventually converge to a particular level as the input power increases. Therefore the curves become flatter and flatter. Another observation is that, the saturation power increases as the biasing current grows. Saturation point is the point where the gain of SOA decreases from the small

signal gain by 3 dB. As indicated by the curves, the saturation input power is 1.5 mW when the biasing current is 120 mA, while the corresponding saturation output power is 16 mW. However when the biasing current increases to 220 mA, the input power saturate at 2.1 mW, and the corresponding saturation output power is 31 mW.

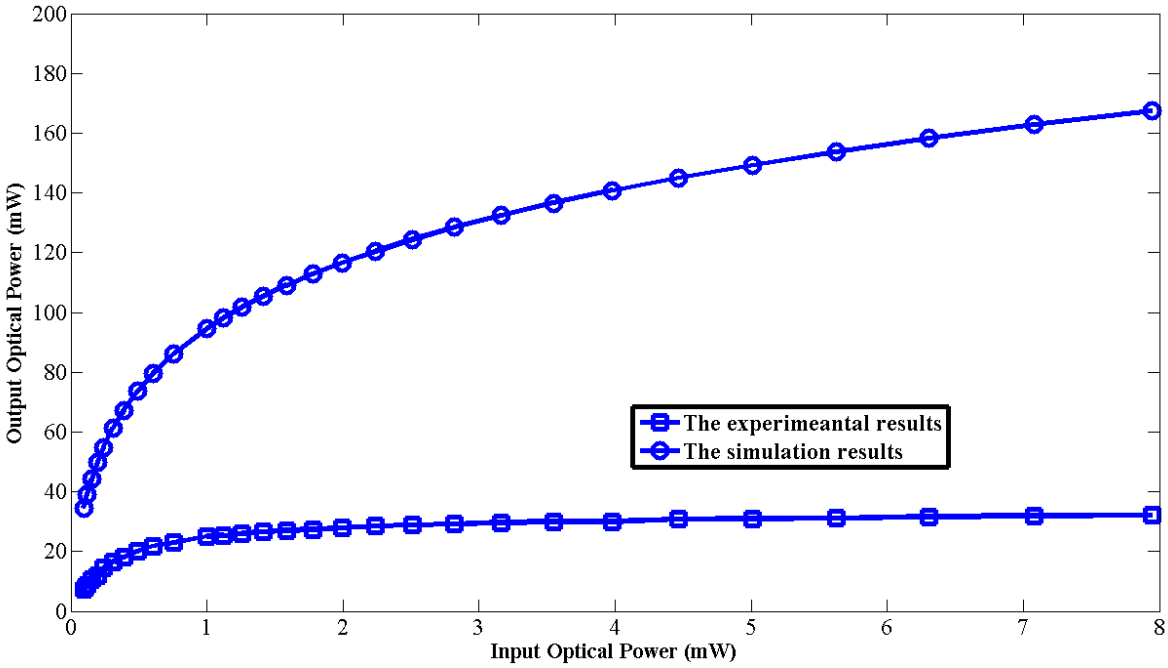

Fig. 2.6: Simulation results compared with experimental measurements

Referred to the specifications of our SOA, we chose the following parameters to calculate the output power, $G_0 = 792$， $P_{sout} = 31\text{mW}$， $L = 1.5\,\text{mm}$, when the SOA is biased with 200mA constant current. The simulation results compared with the experimental measurements are shown in Fig. 2.6. Circles represent the simulation results based on the

equation 2.8, while the squares stand for the experimental measurements. It is surprise to find the significant difference between them so that we believe that the existing formula cannot exactly describe the SOA gain characteristics at saturation region. The theoretical calculations are much larger than the experimental measurements. In addition, the saturation effect is not obvious for theoretical calculations. Consequently, a modification is necessary to make the equation 2.8 more accurate in practical application.

2.4 Theoretical modification

In this section, we perform an investigation and thus theoretical modification to the well-known formula in order to get a more accurate description of SOA gain characteristics.

In an SOA, electrons (more commonly referred to as carriers) are injected by an external current source into the active region. The carrier density at position z in the amplifier can be described by equation 2.9 [66]. The carrier density rate equation 2.9 assumes that the carrier density is nearly uniform in the transverse direction and the bias current is assumed to have a uniform distribution across the active region width.

$$\frac{\mathrm{d}N}{\mathrm{d}t} = \frac{I}{qV} - \frac{N}{\tau_c} - R_{st}P \tag{2.9}$$

where N is the carrier density, I is the injected current, q is the charge of the electron, V is the volume of the active region, τ_c is the carrier lifetime, R_{st} is stimulated emission coefficient, P and is the injection power. The first term on the right hand side (RHS) represents the additional carriers in the active region result from the bias current. The second term is due to the radiative spontaneous emissions and other non-radiative recombination mechanisms. The third term on the RHS represents radiative recombination of carriers for net optical gain.

The variation of photon number is determined by three sources inside the active region. First, the stimulated emission will increase the photon number. Second, material absorption will decrease it. Last, the spontaneous emission will also increase it. Since the photon number is directly related to the power, thus we can get:

$$\frac{\mathrm{d}P}{\mathrm{d}t} = R_{st}P - \frac{P}{\tau_p} + P_{\mathrm{sp}}\Delta\upsilon \tag{2.10}$$

where τ_p is the average photon lifetime in the amplifier cavity, P_{sp} is spontaneous emission coefficient, $\Delta\upsilon$ is ASE bandwidth. For a photon, the relationship $t = z/v$ is always fulfilled. z is the distance along the length of SOA active region, and v is the velocity of photons inside the active region. Therefore we can derive equation 2.11,

$$\frac{\mathrm{d}P}{\mathrm{d}z} = \frac{R_{st}}{v}P - \frac{P}{v\tau_p} + \frac{P_{\mathrm{sp}}}{v}\Delta\upsilon \tag{2.11}$$

where $R_{st}P/v$ stands for the stimulated emission. $P/(v\tau_p)$ indicates the absorption loss, while $P_{sp}\Delta\upsilon/v$ is the ASE noise results from the spontaneous emission. If we ignore the effects of absorption loss and spontaneous emission, we can obtain equation 2.12:

$$\frac{\mathrm{d}P(z)}{\mathrm{d}z} = gP(z) \tag{2.12}$$

where $g = \frac{R_{st}}{v}$. In case of continuous wave amplification (pulse width τ >>carrier lifetime τ_c) and the wavelength of the injected optical signal is near the gain peak wavelength of the SOA, the gain coefficient g can be written as [67]:

$$g = \frac{g_0}{1+(P/P_{\mathrm{s}})} \tag{2.13}$$

From equation 2.13, we can easily obtain equation 2.8. Therefore equation 2.8 does not take the absorption loss into account. Since the spontaneous emission part $P_{sp}\Delta\upsilon/v$ in

equation 2.11 is a wide-band noise [68], it can be suppressed by an optical band-pass filter. Then we can set the absorption loss coefficient to [69]:

$$\alpha = \frac{1}{v\tau_p} \tag{2.14}$$

It is at the order of $10^3 / \mathrm{m}$ [70]. Thus it can be neglected in case of small injection power as the gain is much larger. But it is comparable to gain when the SOA is in saturation region as the gain decreases. Thus equation 2.12 becomes:

$$\frac{\mathrm{d}P(z)}{\mathrm{d}z} = (g - \alpha)P(z) \tag{2.15}$$

Substitute equation 2.13 into equation 2.15, and set the boundary conditions to: $P(0) = P_{in}$, $P_{out} = P(L) = GP_{in}$, we can get the new formula for the gain characteristics:

$$G(dB) = 10\lg\frac{P_{out}}{P_{in}} = 4.34L(g_0 - \alpha) + 4.34\frac{g_0}{\alpha}\ln\frac{g_0 - \alpha - \alpha\dfrac{P_{out}}{P_s}}{g_0 - \alpha - \alpha\dfrac{P_{in}}{P_s}} \tag{2.16}$$

The left hand side (LHS) in equation 2.16 is the gain in dB. Setting $\alpha = 2000/m$ [71-72], $g_0 = 4449/m$ ($G_0 = 792$), the triangles curve in Fig. 2.7 is obtained. The saturation effect is quite obvious in the triangles curve obtained through the revised formula. The revised calculations are lower than the experimental results at a smaller optical power injection.

We believe that the carrier distribution inside SOA should be non-uniform. However, for simplicity we treat the carrier distribution as uniform. Thus our theoretical results are smaller before saturation. Fig. 2.7 illustrates the simulation results based on our proposed equation together with simulation results based on equation 2.8 compared with experimental measurements. From the graph, we can clearly tell that the simulation results based on the proposed revised formula agree with experimental measurements better. The predicted saturation point from the revised formula is much closer to the experimental measurements comparing with saturation point obtained from original formula.

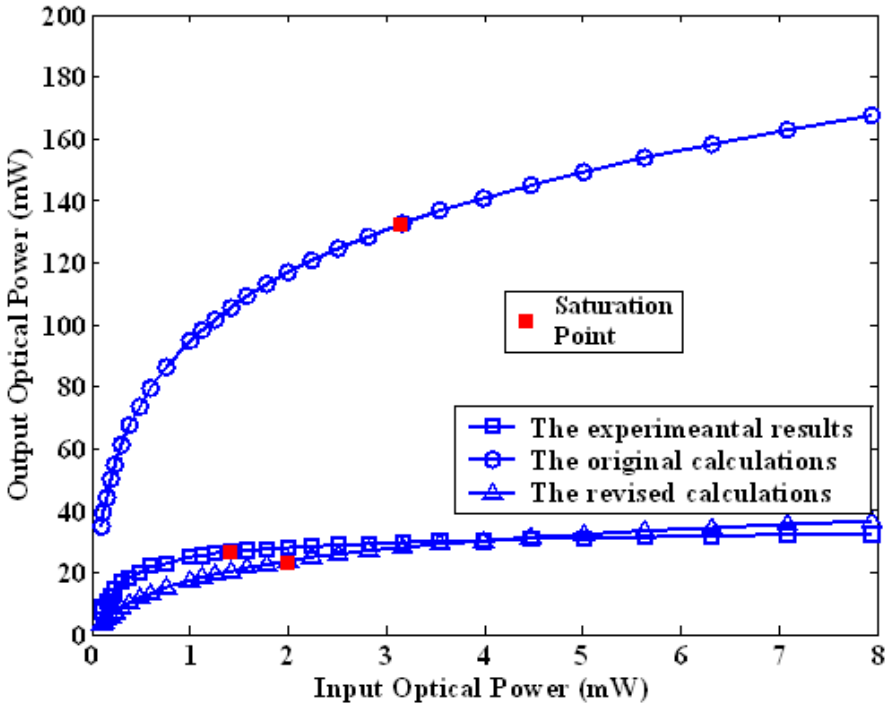

Fig. 2.7: The measured and calculated gain curves for the Kamelian SOA (biasing current: 200 mA)

Fig. 2.8 shows the normalized gain G/G_0 with respect to the input optical power. The circles represent the original calculation based on equation 2.8, while the squares curve stands for the results obtained from our equation. As we can see, the squares curve is much smaller than the circles curve, and it is closer to the experimental results in the saturation region. Although G.P.Agrawal *et al.* has already considered the effect of absorption loss in their SOA model[73], our proposed equation is much simpler. That is because all the parameters in equation 2.16 can be easily obtained by experimental measurements.

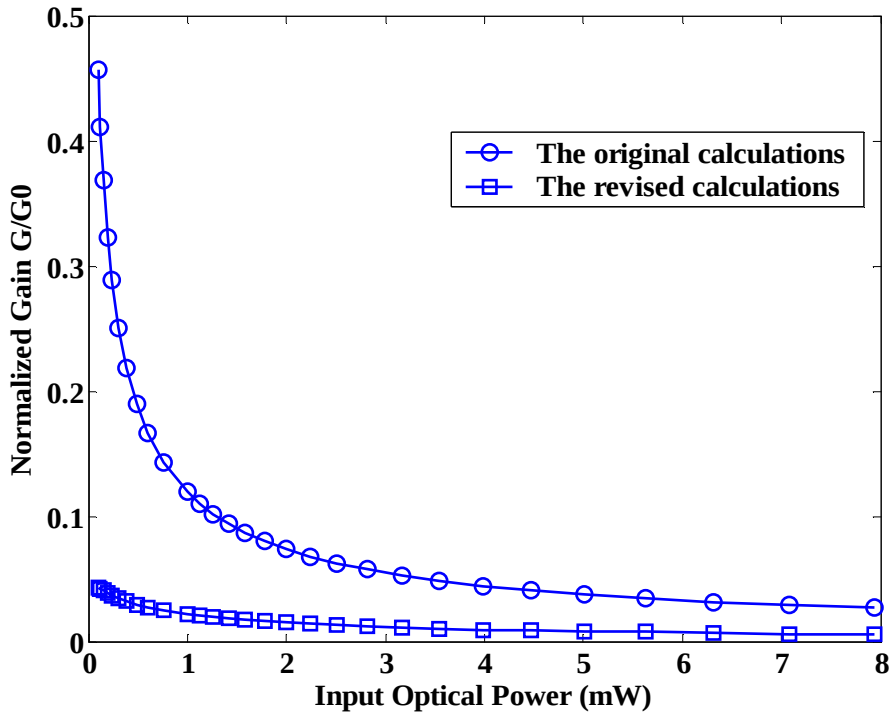

Fig. 2.8: Normalized gain curves for the Kamelian SOA (biasing current = 200 mA)

To justify that our equation can be applied to other SOAs, we measure another SOA from Inphenix with the same experimental setup. The small-signal gain of this SOA is 131, when it is biased at 100mA. The simulation parameters are chosen as following: $\alpha = 2000/m$, $g_0 = 4431/m$, $L = 1.1mm$, and $P_{sout} = 25mW$. The circles in Fig. 2.9 represent the results obtained through the original equation 2.8. The squares are the experimental results. And triangles stand for the results based on our revised formula. Although there is still small difference between our revised calculations and the experimental results in Fig. 2.9, the accuracy is greatly improved. Thus we confirm that our modification can be also applied to other SOA.

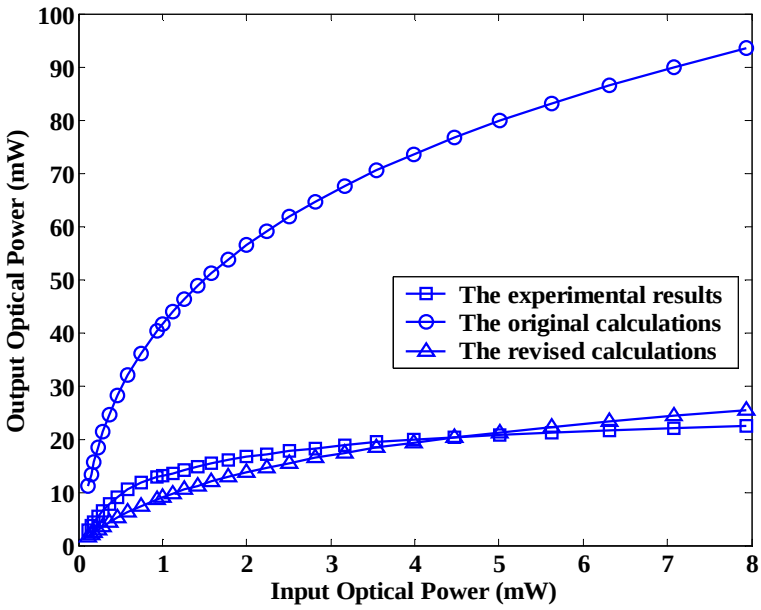

Fig. 2.9: The measured and calculated gain curves for IHPHENIX SOA (biasing current 220 mA)

2.5 Conclusions

SOA is a key device for future all-optical network. The gain characteristics of SOA should be widely concerned in all SOA-based applications. However, there is a significant discrepancy between the experimental results and the results calculated from the widely used equation. Our investigation indicates that the discrepancy resulted from the neglect of the absorption loss, which is insignificant in case of small signal amplification. However it cannot be ignored when the SOA is operated at the saturation region. A modification to the common-use SOA gain formula is proposed by taking the effect of the absorption loss into account. The experimental measurements confirm the feasibility of our modification which can be applied to various types of SOA.

Chapter 3 All Optical Buffer based on Nonlinearities in Semiconductor Optical Amplifier

3.1 Introduction

In this chapter, a loop type fiber delay line optical buffer based on nonlinear polarization rotation (NPR) in SOA is proposed and investigated. Section 2 illustrated an all-optical switch based on NPR in SOA. Experiments have been carried to verify the feasibility of the proposed all-optical switch. Section 3 demonstrates an all-optical buffer based on the all-optical switch proposed. Investigations on microwave signal storage and data packet storage have been carried out. Finally, section 4 summarized the chapter.

3.2 All-optical Switch based on Nonlinear Polarization Rotation (NPR) in SOA

3.2.1 Schematic and operation Principle

This section elaborates the detailed operation principle for NPR, followed by proposed all-optical switch schematic.

3.2.1.1 Nonlinear polarization rotation with linear polarization maintenance

Nonlinear polarization rotation is caused by birefringence introduced by any waveguide. In an SOA, the carriers consumed in active region provide amplification and amplified spontaneous emission (ASE) noise. By adjusting the biasing current or injected optical power, the carriers' distribution inside the active region varies. Thus, the birefringence introduced into the active region is altered. Consequently, the polarization state of the signal output from the SOA changes. This can also be explained by the evolution of the electric field. The electric field can be decomposed into two orthogonal components transverse electric (TE) and transverse magnetic (TM). TE and TM components will experience difference gain and phase change as the light travels along the SOA. As a result, the overall polarization state of the light (resultant of TE and TM components) will

change. Fu, et al, [74] proposed a geometrical model to describe the process of NPR in SOA with negligible polarization dependent gain (PDG). By using this method, two orthogonal polarization states can easily be found; the NPR process can then be maintained along the equator of the Poincaré sphere (PS). The idea can be easily testified by schematic present in Fig. 3.1.

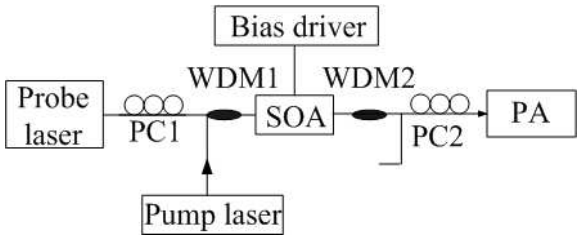

Fig. 3.1: Schematic diagram (PC: polarization controller; PA: polarization analyzer; WDM: wavelength division multiplexer)

The SOA is biased at a constant current level. The input power of probe laser is fixed also. By gradually increasing the power of the pump laser, the polarization state of the probe signal will change after coming out from the SOA. As observed on the PS, a circular track is formed as the pump power changes. By adjusting PC1, the radius of the circular path is gradually reduced. When the circular track reduces to a given point on the PS, the output polarization state from the SOA will not change with varying pump power. PC2 is then carefully adjusted to move that point to the north pole of the PS. Afterwards, the point is moved to the equator of the PS by adjusting the PC1. Finally, we gradually change the pump power, and the output polarization state evolves along equator of the PS. An 180^{o}

azimuth rotation can be easily achieved by tuning the pump power over a specific range. This is the basic idea of linear polarization state maintenance during the NPR process. Fig. 3.2 presents the process with the help of the PS. The output SOP will travel along the equator of the PS from H position to V position. Thus polarization switching between the vertical linear SOP (V position on the PS) and the horizontal linear SOP (H position on the PS) can be obtained. Then a polarization beam splitter (PBS) can be used to perform the polarization-to-intensity conversion, the packet signal will be switched between two output ports (V port and H port) of the PBS.

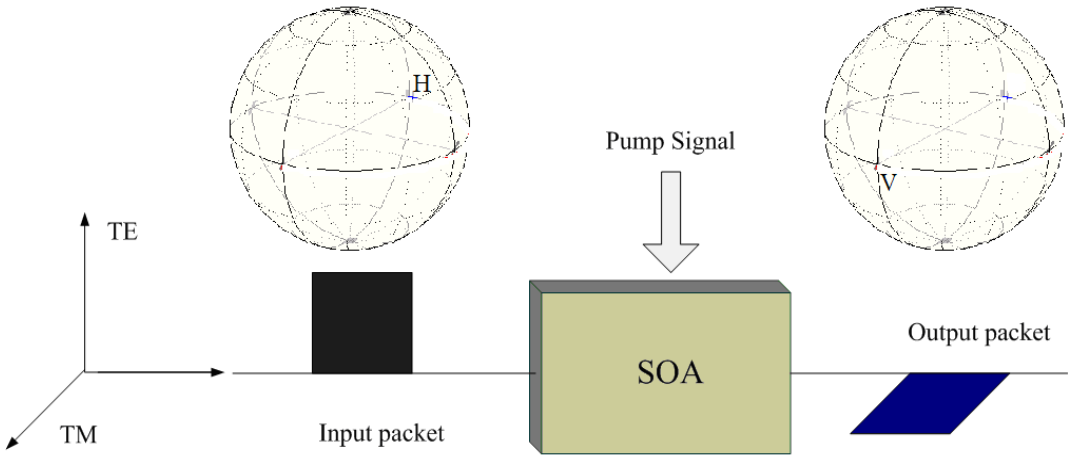

Fig. 3.2: The process of NPR arising in SOA

3.2.1.2 Proposed all-optical switch schematic

Based on the NPR process discussed in the previous section, we proposed a new schematic for all-optical switch. And we experimentally verify it. The experimental set up is illustrated in Fig. 3.3.

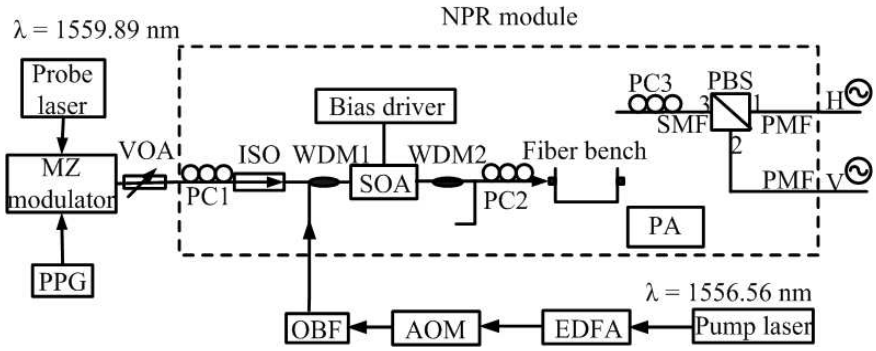

Fig. 3.3: Experimental set up of all-optical switch (PMF: polarization maintaining fiber; SMF: single mode fiber)

A distributed feedback (DFB) laser source is used to generate a continuous wave (CW) probe light at 1559.89 nm with maximum 10 dBm output power. Next, a digital data packet imposed on the optical carrier is generated by a Mach-Zehnder (MZ) intensity modulator driven by a 2.5 Gb/s pseudorandom binary sequence (PRBS) with a word length of 2^{15}-1 generated by the pulse pattern generator (PPG). The output power of the input signal is adjusted by a variable optical attenuator (VOA). The polarization-dependent gain (PDG) of the CIP SOA (SOA-L-OEC-1550) is 0.5 dB and the peak gain wavelength is 1520 nm when the SOA is biased at 500 mA and thermally stabilized at 20°C. Two wavelength division multiplexers (WDMs), with a pass-band of 0.8 nm are used to introduce/remove the control light into the SOA by forward pumping scheme. The

pump laser, operating at 1556.56 nm, is provided by another DFB laser source with a maximum output power of 13 dBm, whose output power is further amplified by an erbium-doped fiber amplifier (EDFA). It is then modulated by an acoustic optical modulator (AOM) driven by a 250 kHz square wave to provide an optical control signal. A tunable optical band-pass filter (OBF) with 1 nm bandwidth is used to reject excess noise coming out from the EDFA. The optical isolator (ISO) is used to ensure unidirectional propagation and suppress undesired reflections. The detection head of the polarization analyzer (PA) (Thorlabs PA430) is coupled to the output of SOA by a fiber bench in order to measure the SOA output polarization state of the probe light accurately. Next, after replacing the PA with the polarization beam splitter (PBS) and adjusting the PC3 to keep the polarization trajectory consistent, the all-optical switch is achieved experimentally. As the two outputs ports of PBS correspond to two orthogonal linear polarization states, the initial polarization state of probe light is aligned with that of H port of the PBS. By gradually increasing the pump power, the polarization state of the probe light will gradually change, thus the probe light comes out from port V of the PBS in the end. By properly setting the pump power variation range, an 180^{o} polarization azimuth rotation along the equator is achieved. As a result, theoretically, all of the probe power will be switched to port V of the PBS.

3.2.2 Experimental results for proposed all-optical switch

3.2.2.1 Linear polarization maintenance

PC1 and PC2 are carefully adjusted so that the polarization state evolves along the equator of PS. The pump power induced NPR with linear polarization maintenance is observed, as shown in Fig.3.4.

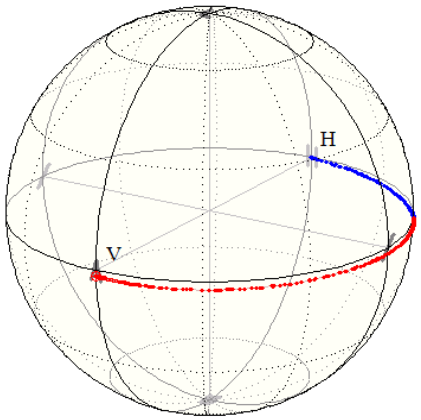

Fig. 3.4: Polarization evolution on the PS

When the output power of the probe laser at 1559.59 nm is kept at 0 dBm, and the SOA biased at 500 mA, a 180° rotation of polarization azimuth of the probe light on the PS can be obtained by increasing the power of CW pump light from -15 dBm to 14 dBm. From Fig. 3.5, we can also see that linear polarization state is maintained during the course of NPR. The ellipticity angle is maintained at nearly 0°, with the degree of polarization at near 100%. The polarization state evolves from horizontal linear polarization state (H

position on the PS) to the vertical linear polarization state (V position on the PS), which are 180^{o} apart from each other along the equator on the PS. As is seen from Fig. 3.5, the azimuth angle difference between them is 90°. This proves that they are orthogonal to each other in Cartesian coordinates. Thus, they correspond to two output ports of PBS, V port and H port.

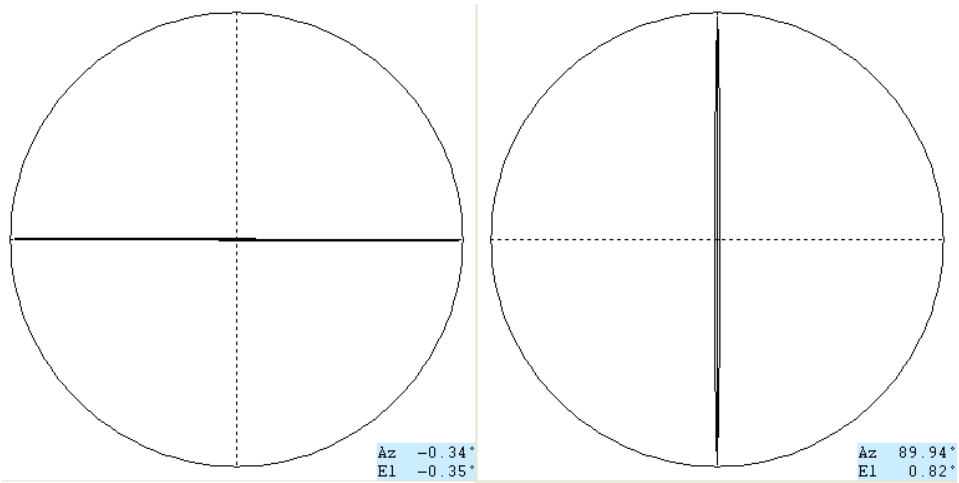

Fig. 3.5: Polarization ellipse (a) Horizontal linear polarization; (b) Vertical linear polarization

3.2.2.2 Pi phase shift

Next, we modulate the pump laser with a 100 kHz sine wave, as shown in Fig. 3.6 (a), while the output power of the probe laser at 1559.59 nm is kept constant at -20 dBm. Two

sine waveforms, complementary to each other, can be observed simultaneously at V port and H port of the PBS, as shown in Fig.3.6 (b) and (c).

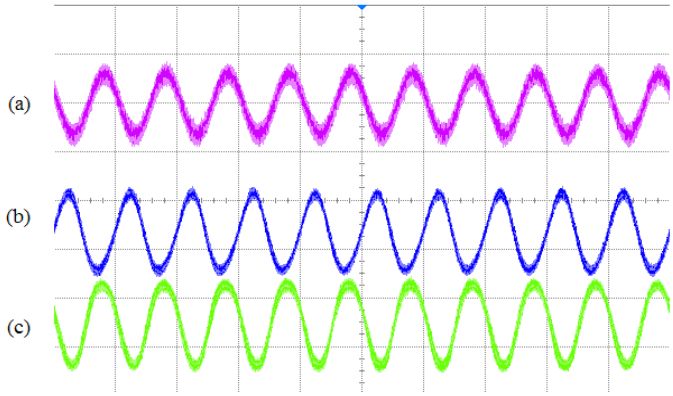

Fig. 3.6 (a): Sine wave input of the pump light; (b): Output waveform of the probe light at H port; (c) Output waveform of the probe light at V port

Both have the same amplitude and frequency. In case maximum pump control signal power happens, the probe light power is at minimum at H port of PBS, while it is at maximum at V port of PBS and vice versa. This indicates that the pump control signal could switch all of the probe power from one port to another. Thus, we conclude that a π phase shift between the TE and TM components of the electric field is achieved during the course of NPR in an SOA. The phase shift can be set at either 0 or π, according to the power levels of the pump control signal.

3.2.2.3 2.5 Gb/s data packet switching

Finally, pulse patterns of the control and input signal are generated by editing an 80MHz arbitrary waveform generator and a pulse pattern generator (PPG), respectively. Two packets, with 1 μs separation, consist of 500 bytes PRBS at 2.5 Gb/s bit-rate. The width of control pulse is 0.25 μs, in order to cover the first packet (P1). The control pulse is carefully synchronized with the input signal and packet P1 is covered completely, as shown in Fig. 3.7.

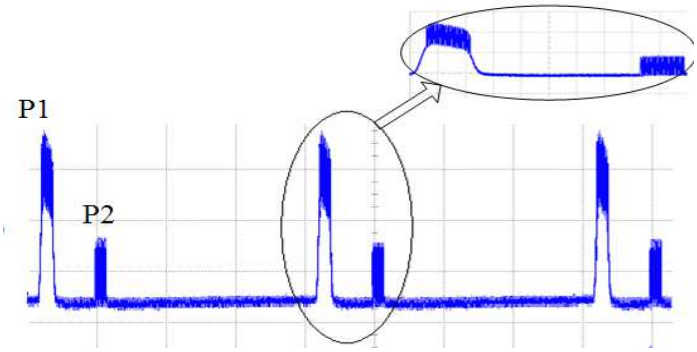

Fig. 3.7: Synchronization of control pulse with P1

The polarization of packet P1 will be changed, while that of packet P2 remains unchanged. The power of control pulse is properly tuned so that a 180° azimuth rotation along the equator of the PS from H position to V position is obtained. The optical control pulse will switch P1 to V port of the PBS, while the second packet (P2) will appear at H port of the PBS. When we monitor the output at the H port of the PBS, it is clear that the amplitude

of P1s is dramatically suppressed when compared with that of P2, as shown in Fig. 3.8 (a). At the V port of the PBS, we observe that it is the opposite case, which is shown in Fig. 3.8 (b). A small power leakage of P2 at V port is observed; this is due to imperfection of the linear polarization maintenance and the inaccurate 180^{o} azimuth rotation. The small dip associated with suppression of P1 at H port results from the cross gain modulation (XGM) effect in SOA. A 20 dB extinction ratio (ER) for the proposed switch is achieved when the pump control pulse with 0 dBm average power is injected.

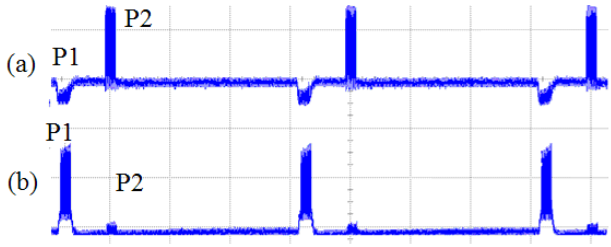

Fig. 3.8: Output waveforms at (a) H port (b) V port

Eye diagrams obtained during the experiment are shown in Fig. 3.9. As we can see, the signal details at H port and V port (3.9 (b) and 3.9 (c), respectively) imply that the input signal patterns are well maintained.

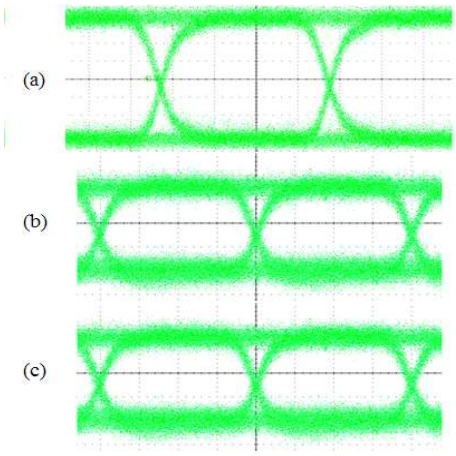

Fig. 3.9 (a): Eye-diagram of input packet; (b): Eye-diagram at output H port; (c): Eye-diagram at output V port

3.3 All-optical Buffer based on All-optical Switch proposed

As we successfully construct an all-optical switch utilizing NPR in SOA, we are going to propose a new schematic of all-optical buffer based on the all-optical switch proposed. The experimental set up is described in subsection 1 and in subsection 2 we investigate the microwave signal storage.

3.3.1 Schematic for the proposed all-optical buffer

As shown in Fig. 3.10, a DFB laser source at 1559.89 nm provides the input probe light. It is modulated by a MZ modulator. The input digital data packet is generated by the PPG and then mixed with a microwave signal using subcarrier modulation technique. The output optical signal is attenuated by a VOA. It then goes into H port (port 1) of a PBS. Port 3 of the PBS is fed into the NPR module shown in all-optical switch scheme. The output port V of NPR module is connected to the V port of the PBS by 10 m PMF to form a loop structure. A pump laser at 1556.56 nm provides the control light. It is then amplified by EDFA and modulated by AOM. Before the control signal is injected into the NPR module, OBF is used to reject excess noise. Output optical signal from the buffer can be converted to electric signal using a photo-detector at H port of NPR module. It is then mixed with a synchronous microwave signals; the bit error rate (BER) measurements can then be taken at the output port of mixer using an error detector (ED).

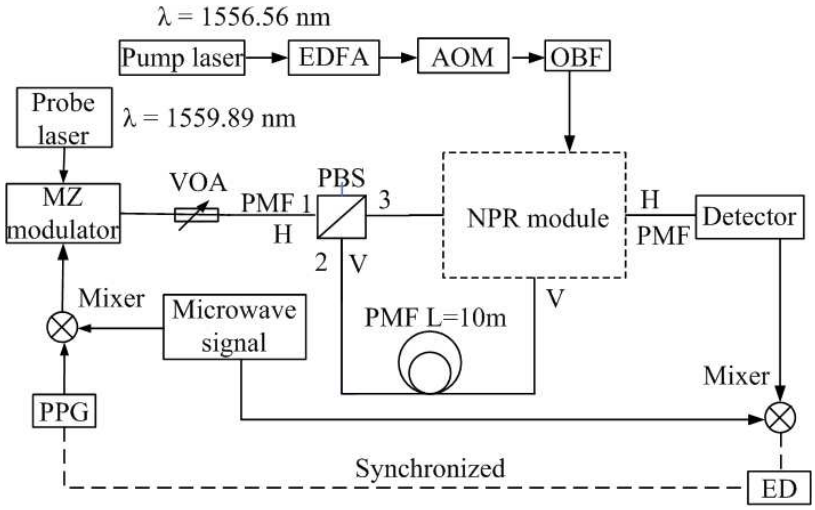

Fig. 3.10: Schematic of proposed all-optical buffer

The NPR module is capable of changing the probe laser's polarization state with respect to the power of pump laser; it has two ports, H and V (correspond to two orthogonal linear polarization states H and V on the PS). The PMF maintains the polarization state of the input signal out from the V port of the switch. On the other end, it is fed into the V port of the PBS to make the polarization state of the input signal inside the loop consistent. The buffer is able to "write/read" signal into/out from the loop. In case of no control signal injection, the NPR module is set so that the input signal launched to the H port of PBS maintains its polarization state and, thus, comes out from H port of the NPR module. As a result, it comes out from the buffer without buffering. Once a properly designed control optical signal is applied to the SOA, the polarization state of the signal changes from initial H position to V position, thus it comes out from port V of the NPR module. The PMF maintains the signal's polarization state; hence, its polarization state matches that of the V port of the PBS. In case no control signal is injected afterwards, the polarization state of the input signal remains unchanged when crossing the NPR module. The input signal is therefore, stored inside the loop. To read the signal out, another control signal, which is carefully synchronized with the input signal, is needed to change its polarization state when crossing the NPR module back from V position to H position on the PS. The signal comes out from port H of the NPR module, thus, out from the buffer.

3.3.2 Theoretical investigations for all-optical buffer

Due to hardware constraints, we perform theoretical investigations on the all-optical buffer proposed. The parameters of SOA are set as follows: active region length 600 µm, line-width enhancement factor 6.08, optical confinement factor 0.45, and gain recovery time 10 ps. The parameters for PMF are: loss 0.5 dB/km; length 10 m. We are not concerned with the dispersion parameters, as the length here is quite short, thus both chromatic dispersion and polarization mode dispersion effects are ignored. We assume that the total length of others fibers, such as fiber tail for PBS/SOA, is 2 m. As a result, the fiber loop length is 12 m (this corresponds to 60 ns delay per loop). In this investigation, we set the input digital data packet rate at 2.5 Gb/s.Thus, this all-optical buffer scheme is able to handle data packets with length up to 150 bits. This is calculated in the case when the last bit just enters the PMF, and the first bit is about to leave PMF.

3.3.2.1 Varying SOA biasing current

First, we fix the input signal power and control signal power and change the value of SOA biasing current to observe its effect on the buffering results. From previous experimental results [74], we know that, for an input power of -20 dBm, a control power of 16 dBm dynamic will induce 180^{o} azimuth rotation under 200 mA biasing current. Because of this, we fix the input power at -20 dBm and control power at 16 dBm. We then increase the current from 50 mA to 350 mA. The PPG generates 2.5 Gb/s pseudo random bit sequence

(PRBS) digital data packet, which is then mixed with a 10 GHz sine microwave signal. We take the bit error rate (BER) after the received signal is electrically mixed with a synchronous microwave signal with the same frequency for buffering results after 5 cycles.

The results are illustrated in Fig. 3.11. As we can see, a 200 mA biasing current provides the best results. In case of a biasing current of less than 200 mA, the amplification the SOA provides to the input signal is smaller. Moreover, the polarization azimuth rotation is more than 180^{o}. As a result, the ER of polarization switching is degraded when the packet is passed through the PBS. In case of a biasing current larger than 200 mA, the polarization azimuth rotation is less than 180^{o}. Consequently, a larger loss is encountered when the signal passing through the PBS. This also proves that the polarization azimuth rotation is the key factor to signal quality.

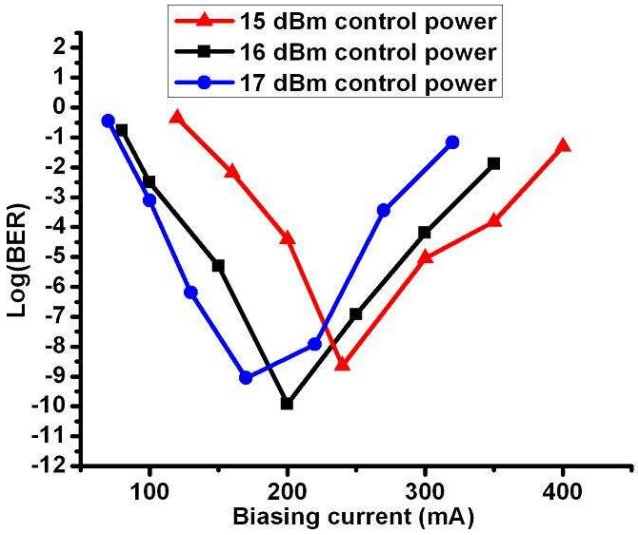

Fig. 3.11: BER measurements under different biasing current (packet data rate 2.5 Gb/s, microwave signal frequency 10 GHz)

Next, we reduce the control power to 15 dBm. The biasing current giving the best results shifts to 240 mA. In order to get an 180^{o} polarization azimuth rotation, the SOA needs to be supplied with a larger biasing current. The results though, are not as good as 16 dBm control power case; this is because the larger biasing current and the lower control power give a higher ASE noise. When we increase the control power to 17dBm, the optimum biasing current reduces to 170 mA. We also notice this phenomenon in the experiments on all-optical switch. If the control power is larger than 16 dBm, we could not achieve an 180^{o} polarization azimuth rotation. This is because the large control power consumes most of the carriers. Although the consumed carriers could be supplied by increasing biasing

current, the active region cannot take all the carriers injected. Thus the impact of biasing current on the polarization change becomes weaker.

3.3.2.2 Varying control power

Next, we will examine the effect that the control power has on buffering results. We fix the input signal power at -20 dBm and the SOA biasing current at 200 mA. We also increase the control power from 11 dBm to 21 dBm and still take the BER measurements for buffering of 5 cycles. The frequency of the microwave signal and the data rate of the digital data packet remain unchanged.

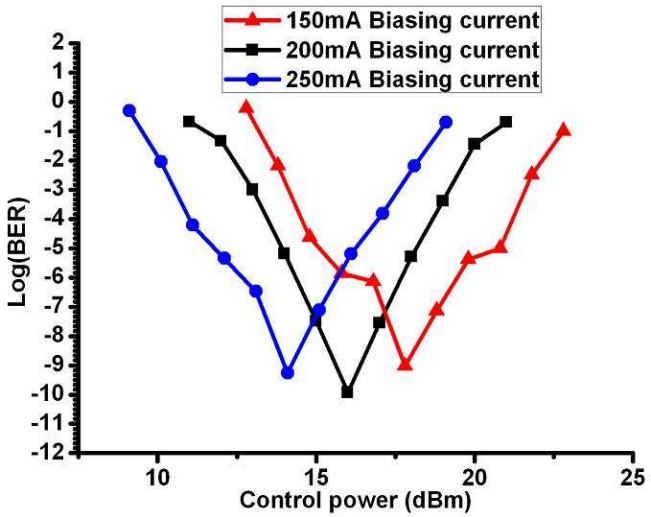

Fig. 3.12: BER measurements under different control power (packet data rate 2.5 Gb/s, microwave signal frequency 10 GHz)

As observed in Fig. 3.12, the control power that gives largest polarization azimuth rotation provides the best buffering results. At smaller control power, the input signal suffers a larger loss when crossing the PBS. And this is due to the imperfection of the polarization azimuth rotation. When the control power exceeds that value, the SOA will be saturated. Thus, the control signal consumes more carriers, which results in a smaller input signal gain. A polarization azimuth rotation larger than 180^{o} also degrades the performance of the proposed scheme.

If we reduce the SOA biasing current to 150 mA, the control power needs to achieve 180^{o} polarization azimuth rotation increases from 16 dBm to 17.8 dBm. The smaller gain provided by SOA however, affects the buffer performance. As more carriers are consumed by the control signal, there are less left for amplification of input signal. In the case of 250 mA SOA biasing current, the best case control power decreases to 14.1 dBm. This is because the large biasing current generates large ASE noise. And the large ASE brings down the scheme performance.

3.3.2.3 Varying input signal power

In the next step, we change the value of input signal power from -25 dBm to -15 dBm. The control power is fixed at 16 dBm and the SOA biasing current is fixed at 200 mA,

initially. We still take the BER measurements after 5 cycles buffering; other conditions remain unchanged.

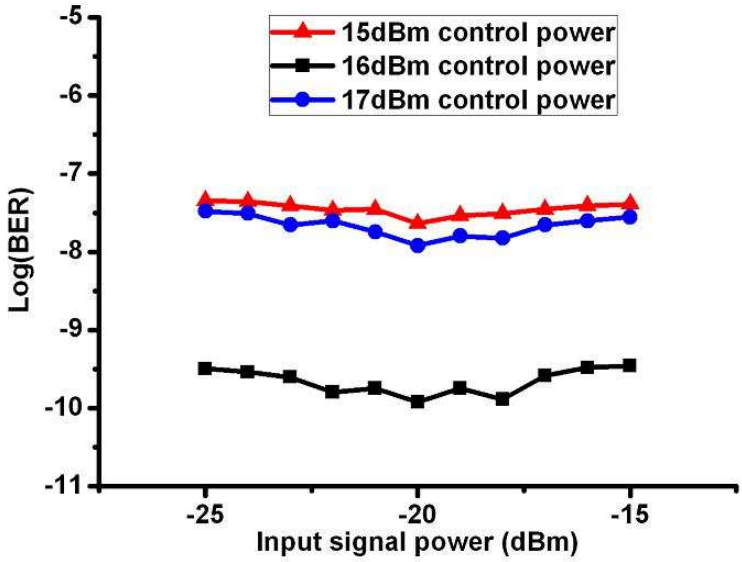

Fig. 3.13: BER measurements under different input signal power (packet data rate 2.5 Gb/s, microwave signal frequency 10 GHz)

From Fig. 3.13, we notice that the input signal power has almost no influence on the buffering results when the control power and biasing current is fixed. The control power still strongly affects the buffering results. This is because the input signal power is very small when compared to the control signal power. The input signal power change could affect its polarization as the increasing signal power consumes more carriers. Thus the active region shape will change. Eventually, the input signal polarization changes. But as

we are going to make use of the polarization change induced by control signal, we have to minimize the impact of input signal power. This diagram also proves that, a signal power fluctuation from -25 dBm to -15 dBm has little impact on the buffering results.

3.3.2.4 Varying the control signal polarization

We then carry on the investigation by changing the polarization of control signal, while the polarization of input signal is set at 0^o azimuth. In the previous analysis, both signals' polarization is set at 0^o azimuth, and both signals are linear polarized in the beginning, so their ellipiticity is 0. We still take the BER measurements after 5 cycles buffering as judgment criteria, while other conditions remain the same. The results are shown in Fig. 3.14. Obviously, the polarization of the control signal power almost doesn't affect the buffering results. The BER measurements fluctuation in log scale is less than 0.7 and the value is below 10^{-9}.

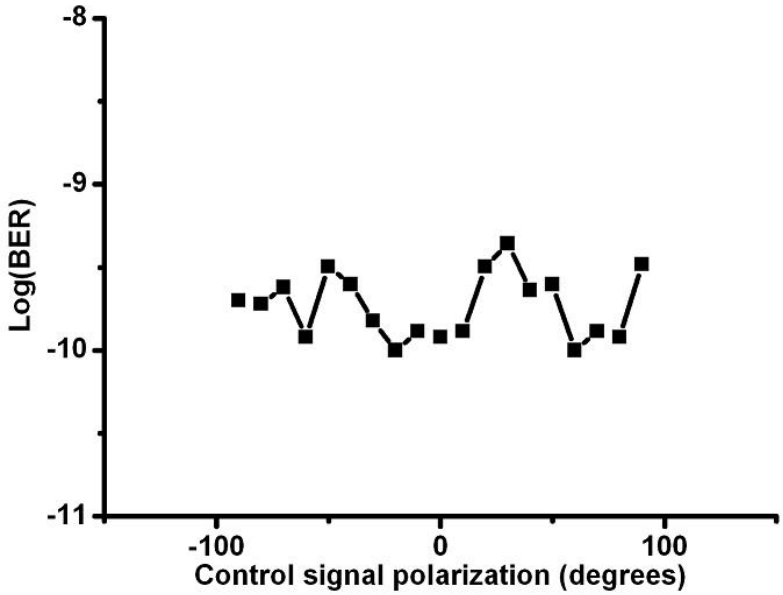

Fig. 3.14: BER measurements under different control signal power polarization (packet data rate 2.5 Gb/s, microwave signal frequency 10 GHz)

3.3.2.5 Negative control signal

In the investigations performed above, the control signal is in positive format. This means the control signal is high when it overlaps with input signal which needs to be buffered to induce the polarization state change, but it is low otherwise. While there are draw backs for this technique, high control signal power (bits “1”) may induce cross gain modulation （XGM） on the buffered input signal. Additionally, low control signal power (bits “0”) cannot consume enough carriers in SOA. As a result, the output ASE noise from SOA is high. So a negative control signal format is introduced. It is low when it overlaps with

input data packet, which needs to be buffered; otherwise it is high. This idea is illustrated by Fig. 3.15.

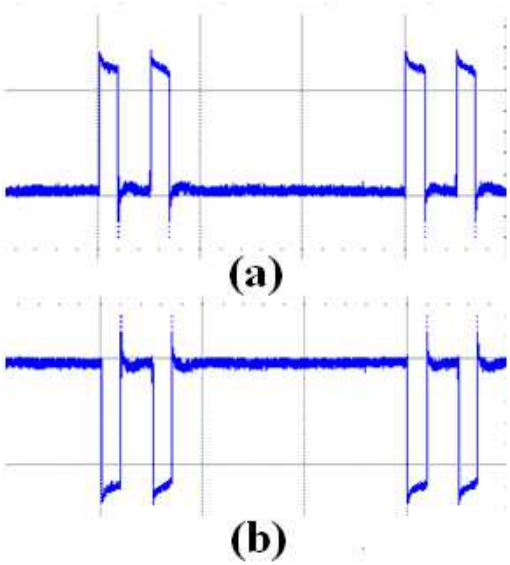

Fig. 3.15 (a): Positive and (b): negative control signal format

The SOA is biased at 200 mA with the input signal power at -20 dBm. The control signal power is 16 dBm, with negative control format. We take BER measurements after buffering from 1 to 20 cycles and compare with positive control signal format. The results are presented in Fig. 3.16.

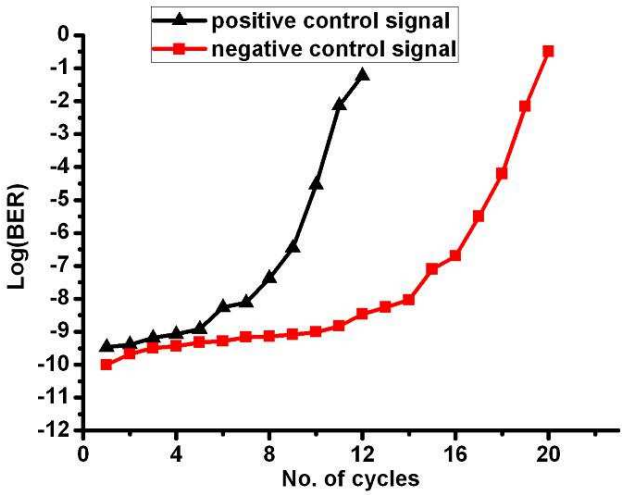

Fig. 3.16: BER measurements under positive and negative control signal (packet data rate 2.5 Gb/s, microwave signal frequency 10 GHz)

The curves prove the feasibility of the proposed negative control signal. The control signal depletes the SOA to depress the ASE noise, and it reduces the XGM effect on the input data packet to give the input signal a larger gain. By using positive control signal, the received data is acceptable up to 12 cycles buffering. In case of negative control signal, this number increases to 20. The results also prove that the negative control signal performs better in ASE suppression without sacrificing the impact on polarization azimuth rotation.

3.3.2.6 40 GHz microwave signal buffering

In the earlier analysis, the frequency of microwave signal is 10 GHz. In this section, we perform investigation on the scheme to confirm its feasibility of working with a microwave signal frequency higher than 10 GHz. The input signal power is set at -20 dBm and the control signal power is set at 16dBm with negative format. A 200 mA biasing current is chosen for SOA. The rate of digital data packet generated by the PPG is 2.5 Gb/s. The results are summarized in Fig. 3.17.

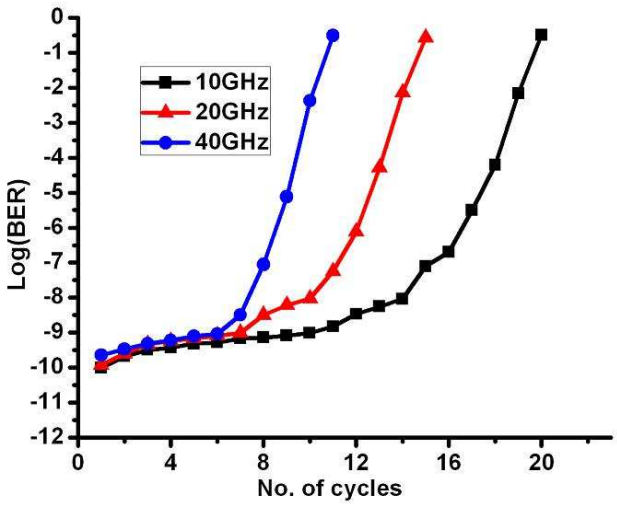

Fig. 3.17: BER measurements for 10, 20 and 40 GHz microwave signal (packet data rate 2.5 Gb/s)

The results in Fig. 3.17 prove that the proposed scheme is able to work under microwave frequency up to 40 GHz. The buffering results do fairly well up to 10 cycles buffering for 40 GHz microwave signal case. Under 20 GHz microwave signal, the digital data packet

is able to be stored for 14 cycles. These results could be limited by the recovery time of the SOA. As the microwave frequency goes higher and higher, the SOA may not respond fast enough.

3.4. Conclusions

In this chapter, a novel scheme of all-optical buffer, based on NPR in SOA for all-optical microwave signal processing, is proposed. The key part of the all-optical buffer, the all-optical switch is first demonstrated experimentally with 2.5 Gb/s digital data packet in optical domain. A linear polarization state is maintained during the NPR process, so that an extinction ratio(ER) of 20 dB is achieved for the proposed switch.

The all-optical buffer, based on the all-optical switch, is then investigated. Effects of input signal power, control signal power, SOA biasing current and control signal polarization on the buffering results are analyzed. We optimized the factors to get the best buffering result. The control signal polarization is studied, as well. A negative control signal format is then proposed to improve the system's performance. It extends the buffering time of 2.5 Gb/s digital data packet mixed with 10 GHz microwave signal from 720 ns (12 cycles) to 1.2 μs (20 cycles). The buffering of 2.5 Gb/s digital data packets, mixed with 20 GHz and 40 GHz microwave signal, are investigated, as well. The output digital data packet, after de-multiplexed with 20 and 40 GHz microwave signal, is maintained well after 840 ns (14

cycles) and 600 ns (10 cycles).The results prove the feasibility of the scheme working with 40 GHz microwave signal. However, due to the generally slow recovery time of SOAs, the data rate of the all-optical buffer scheme is limited. As the data rate keep on increasing, the carriers consumes by the previous packets or bits cannot be completely replaced by injected carriers into the active region. Thus the gain of SOA will be drained eventually. However, quantum dot (QD) SOA offers a solution to enhance recovery time to a few femto-seconds [75]. There are also other techniques to assist the SOA in reducing recovery time [76]. These could further extend the application of SOA in all optical signal processing.

Chapter 4 Hybrid Amplifier for Wavelength Division Multiplexing (WDM) Passive Optical Network (PON)

4.1 Introduction

In this chapter, a hybrid C+L band fiber amplifier composed of a C-band erbium-doped fiber amplifier (EDFA) and an L-band Raman fiber amplifier (RFA) bridged using double-pass dispersion compensators in a loop-back scheme is proposed first. Using only a single-pump laser diode in this hybrid amplifier, power equalization over the C+L band channels is realized by properly allocating the pump ratio between the C- and L-bands and optimizing the fiber Bragg gratings (FBGs) reflectivity as well as their individual locations in the dispersion compensators for each C+L-band channel. The pump efficiency is improved by recycling the residual pump power whereas the residual amplified C- and L-band channels crossing the other amplifier are blocked by a high isolated C/L-band

WDM coupler. Then we improve the structure to shift single pump laser diode (LD) to wavelength of 1495 nm in order to extend the amplified wavelength to 1610 nm. And bidirectional transmission rather than unidirectional is realized to make it applicable in WDM PONs.

4.2 Bridge-Scheme C+L Band Hybrid Amplifier with Optimum Dispersion Compensation and Gain Equalization

4.2.1 Theory and Proposed Configuration

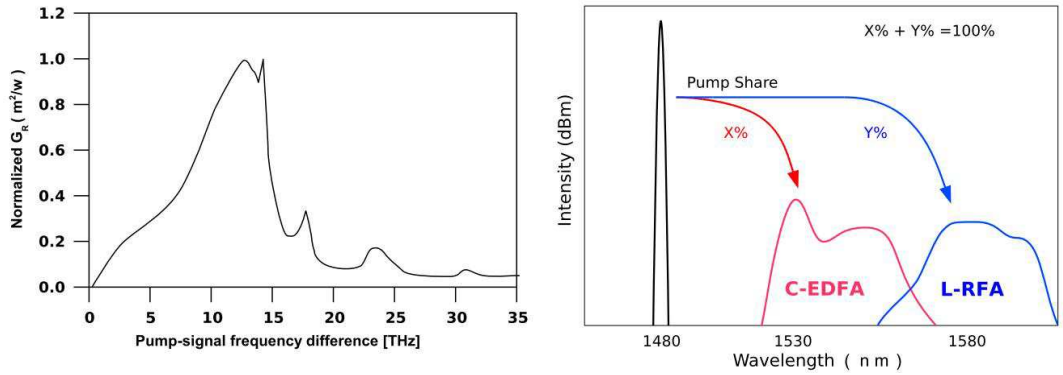

Fig. 4.1(a): The concept of Raman shift; (b): The concept of pump-sharing to C band and L band EDFAs

Stimulated Raman scattering (SRS) is a nonlinear effect occurring in an optical fiber when the propagating light-wave carries high enough optical power. The SRS can extract power from a pump light at shorter wavelength to amplify a weak optical signal at longer wavelength [50]. The Raman shift concept is illustrated in Fig. 4.1(a). Theoretically, if the pump wavelength is located at 1480 nm, the corresponding gain peak in silica-based fibers will come out at the wavelength calculated using the following equation [77]:

$$\Delta\lambda = -\lambda \times \frac{\Delta f}{f} = -\lambda^2 \times \frac{\Delta f}{c} = 94.9nm \qquad (4.1)$$

Where Δf = -13THz and $\Delta\lambda$=94.9 nm are the total amount of detuning with respect to pump frequency and wavelength, respectively. Assuming a single pump laser diode (LD) is used for an L band RFA, the maximum gain will occur at 1574.9 nm. Meanwhile, the C-band EDFA can also be amplified using the same 1480 nm pump LD based on the population inversion mechanism in Er3+ ions. To equalize the gain for both C band EDFA and L band RFA, the pump sharing concept shown in Fig. 4.1(b) could be adopted by appropriately adjusting the pump power ratio of each band.

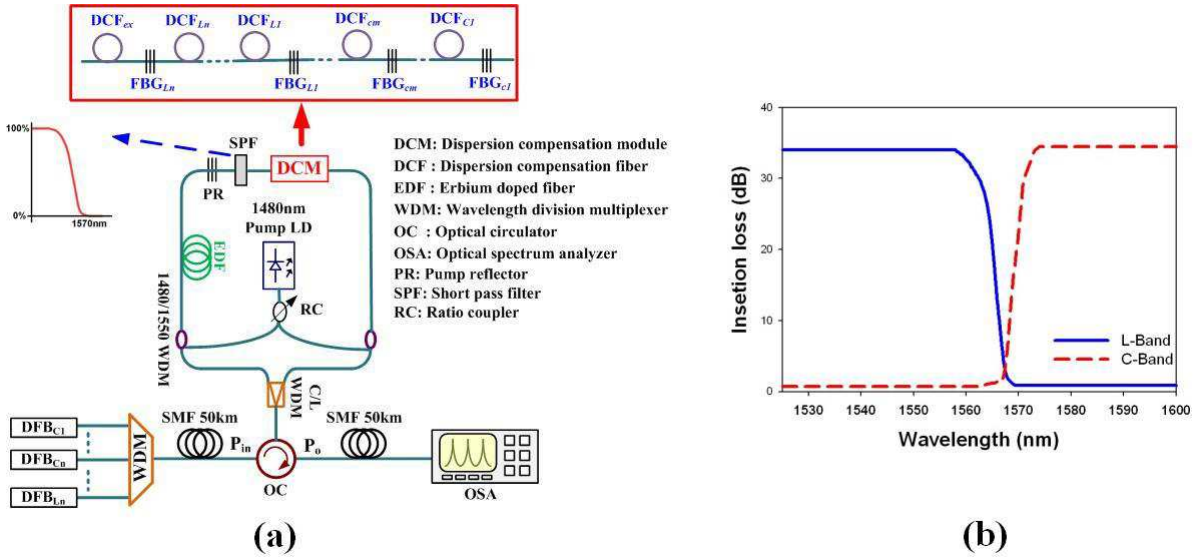

Fig. 4.2(a): Schematic diagram of the proposed C+L band EDFA/RFA; (b): The sideband rejection characteristics of a commercial C+L band WDM coupler

Figure 4.2(a) depicts the configuration of our proposed hybrid amplifier. All C+L band WDM signals go through a 3-port optical circulator (OC) and then are divided using a C/L WDM coupler to enter different loop branches. The C band signals enter the C band branch and then amplified by a forward pump EDFA. A pump reflector is positioned at the EDF end which reflects the residual pump power at 1480 nm for further pumping of this EDF. Meanwhile, the C band signals will go into partial section of the dispersion compensation module (DCM), and then comes back to the EDF again after reflection by the corresponding FBGs. To avoid the residual signal power induces intraband crosstalk by contaminating these original signals, we need to choose a high isolation C+L WDM

coupler with a high side-band rejection ratio to block the residual signals. The specification may refer to a commercial C+L WDM coupler as is plotted in Fig. 4.2(b).

The DCM is composed of several DCF segments in different lengths and several FBGs. Each FBG has a central reflected wavelength matching a separate signal channel. Different signals travel through different DCF lengths, before being reflected by the corresponding FBG to achieve optimum dispersion management for each channel. Note that the path is a round-trip scheme for signals in the DCF to save 1/2 of the DCF length and/or price. The DCM also acts as a double-pass gain medium for L band RFA. To track the signals, for example, a C band signal λ_{Cj} comes from the left hand side of the DCM and travels along the fiber until it is being reflected by the FBG_{cj} ($1 \leqq j \leqq M$) after passing through several DCF segments. After that, λ_{Cj} will return along the same path and be amplified again by the EDF. Finally, this amplified signal will go to the C+L WDM coupler again to enter the output bus strains. On the other hand, an L band signal λ_{Lk} ($1 \leqq j \leqq N$) comes from the right hand side of the DCM and is then being reflected by the FBG_{Lk} after passing through several DCF segments. Similarly, it also passes through the same DCF segments twice and then goes back to the C+L WDM coupler. The DCF length of each segment is varied to precisely compensate the different chromatic dispersions of WDM channels. The Raman pump power travels through all DCF segments, and the residual pump power comes back to the DCM again after being reflected by the same pump reflector used in the C band EDFA. Thus, the pumping power also double-passes

the DCM to improve the pumping efficiency for the L band RFA. Both the C- and L bands signals pass through the common DCF segments of DCM twice for dispersion compensation before being reflected by their corresponding FBGs. After that, the C+L band signals are combined via the C/L WDM coupler and then travel to the same destination (to an OSA) after leaving the 3-port OC. A commercial short-pass filter (SPF) is located after the pump reflector to extinguish the L-band ASE noise generated by the C-band EDFA, so as not to share the Raman gain for L-band signals. The SPF specifications for the 1250-1650 nm tuning range, 58.8 nm/°C tuning efficiency, 55 dB rejection efficiency and 55 dB isolation bandwidth are realizable.

4.2.2 Numerical simulation and Results

The hybrid EDFA/RFA characteristics are theoretically studied in this section. Assuming that there are eight channels ranging from 1530-1565 nm for the C band, and six channels ranging from 1570-1595 nm for the L band, the total pumping power is 640 mW at 1480 nm. In practical applications, the high pumping power could be realized by combining two orthogonally polarized commercial pump lasers using a polarization beam combiner (PBC). To reduce the RFA polarization dependent gain, the 1480 nm pump light could be depolarized before launching into the DCM. To achieve a moderate gain level, the EDF is 6 M in length for the C band EDFA. The Er^{3+} ion, fiber core radius, numerical aperture,

and metastable lifetime are $1.0\times10^{25}(1/m^3)$, 1.4 μm, 0.28, and 10 ms, respectively. The dispersion and dispersion slope of a single mode fiber (SMF) are 17ps/nm/km and 0.058ps/nm^2/km, respectively. The DCF parameter defined here have the same values as those used in [52]. For the following calculation, the input power is -20 dBm for each channel before entering the OC. The estimated output power from port 3 of the OC is 0 dBm for each channel, corresponds to a net gain of 20 dB for the C+L band. The insertion loss of 1480/C+L band WDM coupler, C+L band WDM coupler, and inter-port OC are assumed to be 0.5 dB. These simulation procedures are discussed below:

4.2.2.1 Dispersion management

To describe the simulation process, we use the dispersion map to explain the length of each DCF segment. Fig. 4.3 presents the chromatic dispersion (ps/nm/km) curves both for SMF and DCF in the C+L band region. At 1550 nm, the dispersion and dispersion slope of SMF are 17 ps/nm/km and 0.058 ps/km/nm^2; and those of DCF are -95 ps/nm/km and -0.62 ps/km/nm^2, respectively. The fiber loss for DCF is set at 0.7 dB/km. The dispersion is calculated based on the following formula:

$$D = D_{ref} + \Delta D(\lambda - \lambda_{ref}) \qquad (4.2)$$

And the results are shown in the table below:

Table 4.1: Dispersion profile of SMF and DCF

Wavelength (nm)	Dispersion SMF(ps/nm/km)	Dispersion DCF(ps/nm/km)
1530	15.84	-82.6
1540	16.42	-88.8
1550	17	-95
1560	17.58	-101.2
1570	18.16	-107.4
1580	18.74	-113.6
1590	19.32	-119.8
1600	19.9	-126

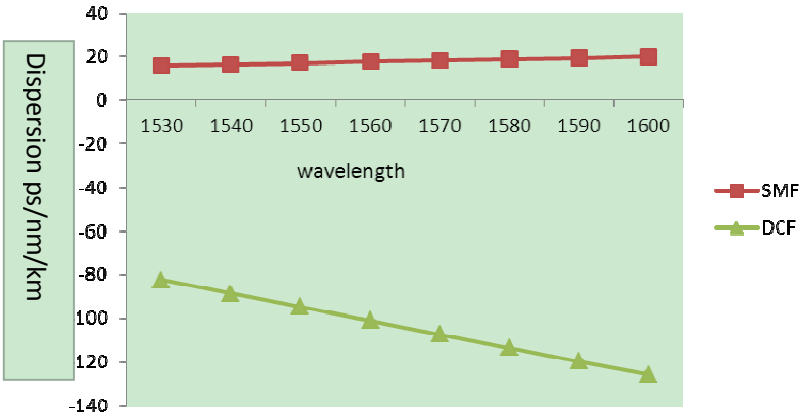

Fig. 4.3: The chromatic dispersion (ps/nm/km) curves both for SMF and DCF

The dispersion compensation using a single segment of DCF could not precisely compensate for all WDM channels. This is attributed to the mismatch in dispersion slope of the DCF and the standard fiber, usually the single mode fiber (SMF). In this work, each signal travel path in the DCF is controlled by a FBG, whose central wavelength is

designed to match the signal wavelength. Each DCF segment length can be predicted based on the following equation:

$$L_{DCF} = -\frac{L_{SMF} D_{SMF}(\lambda)}{2D_{DCF}(\lambda)} \tag{4.3}$$

Where $D_{smf}(\lambda)$ and L_{smf} are the dispersion parameter and the SMF length, respectively, and $D_{dcf}(\lambda)$ is DCF dispersion parameter. Because the WDM signals pass through the DCF twice, there is a 1/2 factor in this expression. To minimize the residual dispersion for WDM channels in a system with 50 km SMF, we find that the required DCF length is 8860 m for the longest wavelength at 1595 nm. It has the minimum dispersion value. As the wavelength decreases, the dispersion value increases. Hence, 8860 m is defined as the common DCF length. Under this condition, the maximum transmission speed R_b of each channel is calculated based on the following equation [77]:

$$R_b = \sqrt{\frac{C}{4 | D_{res} | \lambda^2}} \tag{4.4}$$

Where C is the speed of light in vacuum, D_{res} is the residual dispersion and λ is the central wavelength. To solve this problem, the residual dispersion value is precisely compensated by writing FBGs (FBG_{C1}, FBG_{C2},…FBG_{Cm}, FBG_{L1}, FBG_{L2}, …FBG_{Ln}) at different positions to control the double-pass lengths of DCF for individual signal channel, the residual dispersion can be eliminated exactly. Beside the common DCF length required for all channels, the extra DCF lengths required are 1958, 1697, 1466, 1260, 1075, 908,

757, and 620 m for the C band channels of 1530, 1535, 1540, 1545, 1550, 1555, 1560, and 1565 nm; and these extra DCF lengths needed are 494, 379, 273, 175, 84, and 0 m, respectively, for the L band channels of 1570, 1575, 1580, 1585, 1590, and 1595 nm, respectively.

4.2.2.2 Gain equalization

To implement the gain equalization for C+L band channels, the reflectivity of fourteen FBGs are set as 99% in the beginning before (w/o) gain equalization (GE), as shown in Fig. 4.4(a). Using simulation results from commercial software, we obtain the gain distribution map. The maximum net gain of 27 dB at 1530 nm and the minimum gain of 20.5 dB at 1570 nm are obtained. The gain variation is 6.5 dB among WDM channels. Next, we will equalize the WDM channels by reducing the FBGs reflectance (except that of 1570 nm) to achieve a 20.5 dB net gain as that of 1570 nm. The required FBGs' reflectivities are calculated to be 75%, 70%, 83%, 53%, 18%, 7%, 4%, and 3% for C band channels; and 64%, 50%, 36%, 18%, 26%, and 48% for L band channels, respectively, with 5 nm channel spacing. The gain variation among fourteen WDM channels is reduced to only 0.2 dB after gain equalization. Note that the flattened gain spectrum is as broad as 65 nm over C+L band using only a single pump LD. The splicing loss, including fiber to

fiber, fiber to passive component and FBG sideband loss are less than 0.1 dB in reality. They are neglected in the simulation.

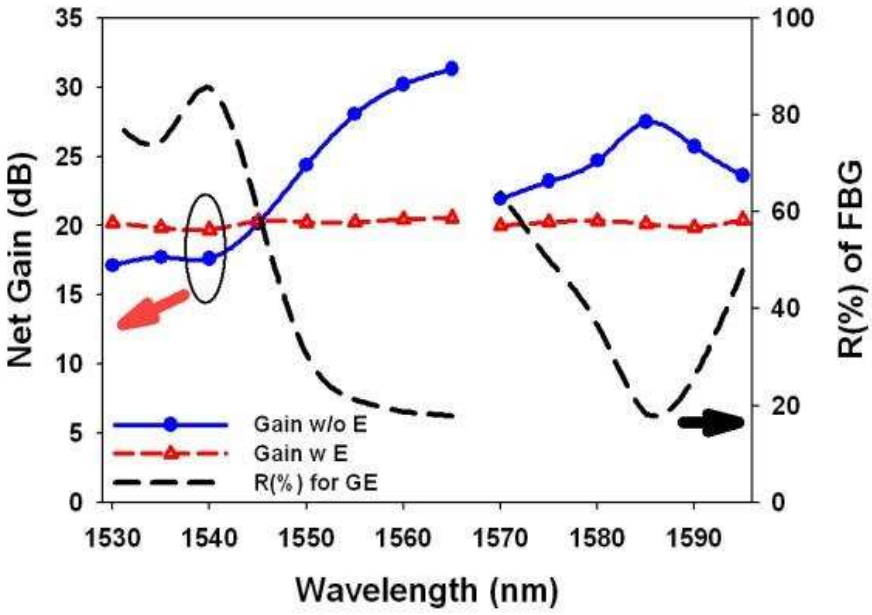

Fig. 4.4: The net gain spectra of C+L-band hybrid amplifier w and w/o gain equalization and corresponding FBGs reflectivities

4.2.2.3 Discussion and Comments

Because the FBGs are designed with different reflectivities for gain equalization purpose, there are residual signal powers for all other 13 channels except for the lowest power channel at 1570 nm. A residual signal power ratio of x% with respect to the original signal

power may penetrate the corresponding FBG if the FBG reflectivity is (100-x) %. The remaining signal power for C band channels will travel clockwise from DCM to 1480/C+L band WDM coupler, and then L band branch of the C+L WDM coupler; while power for the L band channels will travel counter-clockwise from DCM to EDF, the 1480/1550 nm WDM coupler and then C band branch of the C+L WDM coupler. To avoid the residual signal power inducing intraband crosstalk by contaminating these original signals, a C+L band WDM coupler with high side-band rejection ratio is used as mentioned to block the residual signals. The insertion loss is 0.5 dB for each band. The side band rejection efficiency is larger than 55 dB and isolation bandwidth is about 50 nm. A sharp drop at 1567.5 nm produces an extinction ratio large enough to suppress the unwanted noise. Note that the C band branch covers the spectral ranging from 1530 to 1565 nm, while the L band branch is from 1570 to 1595 nm, respectively, in this simulation. When the residual signals enter the counterpart path of the C+L WDM coupler (e.g., L band signals enter C band branch or verse vise), most of the residual signal power will be suppressed. So, the proposed C+L band EDFA/RFA confirms the feasibility of high-quality amplification with negligible intraband crosstalk.

To sum up, this hybrid amplifier has several advantages: (1) The DCF length for chromatic dispersion compensation is almost 50% saved because of double-pass scheme implementation. (2) Dispersion slope mismatch is compensated exactly for all the C+L band channels by writing FBGs at appropriate locations. (3) WDM channels gain variation can be reduced by optimizing the pumping ratio and reflectivity of FBGs from 6.5 dB to

less than ±0.2 dB. (4) The pump efficiency is improved by recycling the residual pumping power using a pump reflector with near 100% reflectivity having the signals passing their gain medium twice. (5) The ASE noise and residual signal power raised from the counterpart band are greatly suppressed by the C+L WDM coupler, making the hybrid amplifier has low NF and negligible intraband crosstalk induced from its own residual signal power.

4.3 Bidirectional Remote-Pumped C+L Band Hybrid Amplifier for WDM PON Transmission

4.3.1 Proposed hybrid pump configuration

The pump sharing concept is illustrated in Fig. 4.5 (a). A single pump LD provides simultaneous pumping for both the C-band EDFA and L-band RFA. The EDFA operates based on a three-level population inversion mechanism, while the RFA operates on Raman shift amplification. If the pump wavelength is 1495 nm, the corresponding gain peak could then be calculated based on the following equation [16].

$$\Delta\lambda = -\lambda \times \frac{\Delta f}{f} = -\lambda^2 \times \frac{\Delta f}{c} = 97nm \qquad (4.5)$$

Where △f = -13THz and △λ=97 nm are the total amount of detuning with respect to the pump frequency and wavelength, respectively. The maximum gain therefore occurs at around 1592 nm in the L band region. To discuss how critical the pump wavelength is to the amplification band, we compare two pump wavelengths of 1480 nm and 1495 nm, respectively. For the 1480 nm pump LD, its maximum Raman gain will occur at 1575 nm, which will lead to a rather low gain level for the longer RFA region. On the other hand, the 1495 nm pump LD will provide enough RFA gain for the 1595-1610 region. Although the longer pump wavelength will degrade the gain for the C band EDFA, the gain is still at an acceptable level for the entire C band.

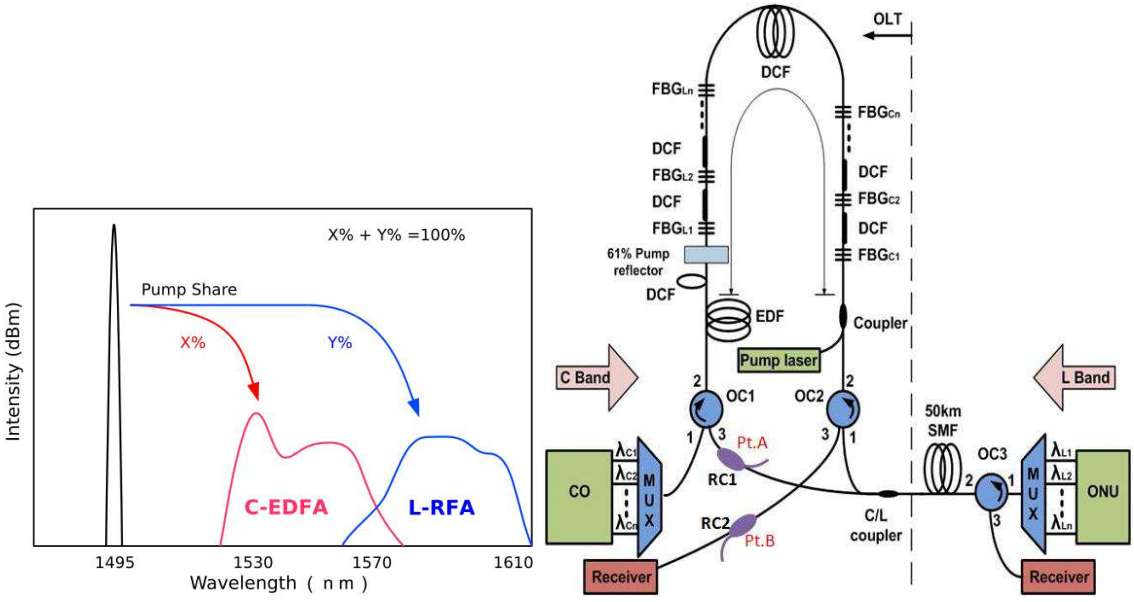

(a) (b)

Fig. 4.5(a): Concept of simultaneously amplified C-band EDFA and L-band RFA using single pumping LD at 1495 nm; (b): The proposed hybrid amplifier (in

between two OCs) and their connection into a 50-km bidirectional WDM PON. (CO: central office, OC: optical circulator, FBG: fiber Bragg grating, ONU: optical network unit).

Fig. 4.5 (b) presents the proposed hybrid fiber amplifier located between two optical circulators (OCs). The hybrid fiber amplifier is then applied in a 50 km WDM PON. 50 km WDM PON means the distance or fiber length from optical line terminal (OLT) to optical network unit (ONU) is 50 km. The system uses different wavelengths for different users. The hybrid amplifier is installed together with the transmitters at the OLT side and there is no active component beyond OLT side. All the dispersion compensation is done on OLT side (pre-dispersion compensation for downlink and post-dispersion compensation for uplink). So we consider this as a WDM PON. The C band signals carry downlink data and the L band signals carry uplink data. And a pair of OCs is used to realize bidirectional operation. The pump light propagates together with the L band signals and provides amplification employing the Raman shift amplification mechanism. After that, the residual pumping power is reflected by a 61% pump reflector, located between the EDF and L band fiber Bragg grating (FBG) array. And the reflected pump light propagates against the L band signal to provide amplification. Bi-directional pumping is used for the L band signals to reduce the RFA polarization dependent gain (PDG) and increase its Raman gain. The rest of the 39% residual pumping power transmits through the pump reflector to provide backward pumping for the C band signals in EDF. This pumping direction will increase the EDFA gain. Moreover, this pumping

direction and ratio distribution will give us optimum gain results for both the EDFA and RFA. Note that the EDFA pumping efficiency is much higher than that for RFA, so only less than 39% of the total pumping power is enough for EDFA gain as compared with the Raman gain. For the optimal dispersion compensation issue, the carefully designed C-band FBG arrays (FBG_{C1}, FBG_{C2} ... and FBG_{Cn}) together with DCF segments will optimally compensate for the chromatic dispersion for all downlink channels. Different downlink channels are reflected back by the corresponding FBGs at different positions, thus, they undergo different DCF lengths. Meanwhile, the L-band FBG array (FBG_{L1}, FBG_{L2} ... and FBG_{Ln}) optimally compensates for the chromatic dispersion of all uplink channels with various DCF lengths. The principle is similar to that of the C-band channels. The pump laser is coupled into the bi-directional hybrid amplifier by a 1495/1550 nm WDM coupler and the C/L coupler separates up and down link data. To suppress the possible leftover C-band signal in the L-band receiver or vice versa, the C band and L band filters may be inserted in front of the L band receiver and C band receiver, respectively. Fig. 4.5 (b) also presents the experimental set-up. In our experiments, we limit the number of wavelengths to 4 to study the feasibility of our proposed system. Ratio coupler 1 (RC1) and ratio coupler 2 (RC2) are used to take measurements from the 4 channels.

4.3.2 Parameters design for simulation and experiment

Both theoretical and experimental works were conducted in this work. For the theoretical study, we simulated 26 channels bi-directional transmission in the WDM PON. They include 13 C-band channels ranging from 1530 to 1565 nm (1530, 1533, 1536, 1539, 1542, 1545, 1548, 1551, 1554, 1557, 1560, 1563 and 1565 nm) and 13 channels in L-band channels ranging from 1570 to 1605 nm (1570, 1573, 1576, 1579, 1582, 1585, 1588, 1591, 1594, 1597, 1600, 1603 and 1606nm), with channel spacing of 3 nm. Four WDM channels with two channels for the C band (1545 and 1553 nm) and the additional two channels (1582 and 1597 nm) for the L band were studied experimentally to prove the feasibility of our scheme.

We keep the simulation parameters consistent with the experimental parameters in order to get accurate description of our system. The following parameters are used in both simulation and experiments. The dispersion parameters for SMF at 1550 nm are 17 ps/nm/km and 0.058 ps/nm^2/km, respectively, while those for DCF at 1550 nm are -95 ps/nm/km and -0.62 ps/nm^2/km, respectively. The EDF density assumes 7×10^{24}/m^3. The meta-stable lifetime is 10 ms and the fiber core is 1.4 μm with numerical aperture (NA) of 0.28 and Er^{3+} ions doping radius of 1.0 μm. The EDF length is 6.0 m. Fig. 4.6 shows both commercial EDF absorption and emission coefficients versus wavelength.

Most of the parameters in this work were selected according to the commercial products which we have in our laboratory. For components consideration, the inter-port insertion loss and isolation loss of OC are 0.6 dB and 50 dB, respectively. The insertion loss for

1495/1550 nm pump coupler is 0.5 dB for each port and 2.5 dB for MUX/DMUX. Using a homemade FBG, the 3-dB bandwidth is less than 0.2 nm and it is out of band (may define as the distance of 30 dB down from peak wavelength) loss of FBG is negligible. The C/L band coupler suppression to each band is 40 dB. The DCF and SMF loss are 0.3dB/km and 0.2dB/km, respectively. The total loss for either EDFA or RFA depends on the total splicing loss and the pumping power and input signal levels. Each FBG is spliced in between DCF segments with a negligible splicing loss of 0.1 dB for each point. The round-trip cascaded loss for FBGs is 0.2 dB (1 ch x 2 times x 0.1 dB) for the shortest distance channel and 5.2 dB (26 ch x 2 times x 0.1 dB) for the longest distance channel, respectively. However, the loss variation issue could be conquered by adjusting each FBG's reflectivity. In the C band the channel at the longest wavelength occurs at 1565 nm and suffers the smallest dispersion. Therefore, it is reflected back first and then travels the shortest distance along the DCF and vice versa for the shortest wavelength channel at 1530 nm. The DCF lengths needed for optimal dispersion for the entire 26 channels for 1530, 1550, 1565, 1570, 1585 and 1605 nm are summarized in the left part of Table 4.1. As the signals double-pass the DCF in the proposed scheme, the length is saved by 50%. The DCF length between the WDM coupler and FBG_{L1} is 8.45 x 0.5 km and the DCF length between the EDF and FBG_{C1} is 9.59 x 0.5 km. The detailed DCF segment length in this proposed scheme is summarized in the right part of table 4.2, with the required DCF length for other wavelengths in between.

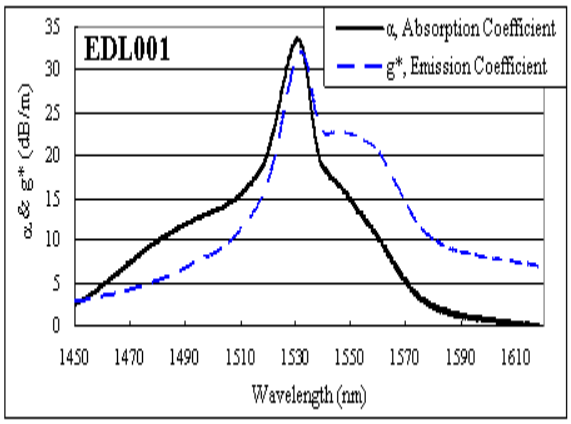

Fig. 4.6: EDF absorption and emission coefficients versus wavelength

Table 4.2: DCF length needed for optimal dispersion compensation

Wavelength (nm)	DCF length (km)	DCF segment	DCF length (km)
1530	9.59	EDF-pump reflector	0.57
1551	8.92	FBG_{L7}-FBG_{L8}	0.026
1565	8.57	FBG_{L12}-FBG_{L13}	0.015
1570	8.45	FBG_{L13}-FBG_{C13}	3.4
1585	8.15	FBG_{C5}-FBG_{C6}	0.046
1605	7.82	FBG_{C12}-FBG_{C13}	0.023

4.3.3 Simulated and experimental results and discussions

Characteristics of hybrid fiber amplifier

We first performed a theoretical analysis on the proposed hybrid amplifier. All of the

channels have an input power of -20 dBm/ch on the CO side. We then used a common DCF segment with a length of 7.82 km for dispersion compensation to all channels. Thus, only the 1605 nm channel is optimally dispersion compensated while the other channels still have residual dispersion. We then used the proposed FBG array together with DCF segments to perform residual dispersion compensation for all of the other channels. The total pumping power is 984 mW in this case. The residual pumping power travels to the pump reflector from the L-band is 162mw, with 61% of residual pumping power reflected back and 39% for (63mW) for C-band EDFA amplification. Without loss of generality, experimental work was also carried out for two C band wavelengths (1545 and 1553 nm) and two L band wavelengths (1582 and 1597 nm), respectively. The 1553 nm distributed feedback (DFB) laser was used instead of 1554 nm (a selected wavelength in simulation) due to a light source shortage in the laboratory. We think the 1553 nm and 1554 nm light source performance should be very similar to their wavelength. Two 1495 nm pumping sources with a total power of 900 mW were combined via a polarization beam combiner (PBC). They were launched into the DCF via a 1495/1550 nm WDM coupler.

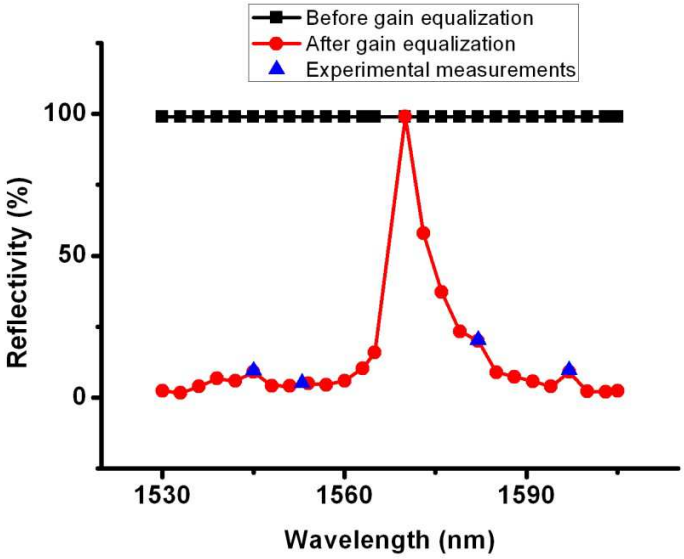

(a)

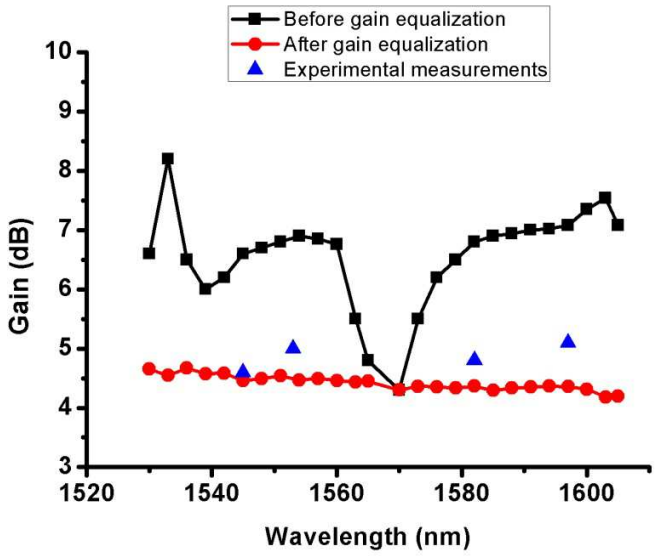

(b)

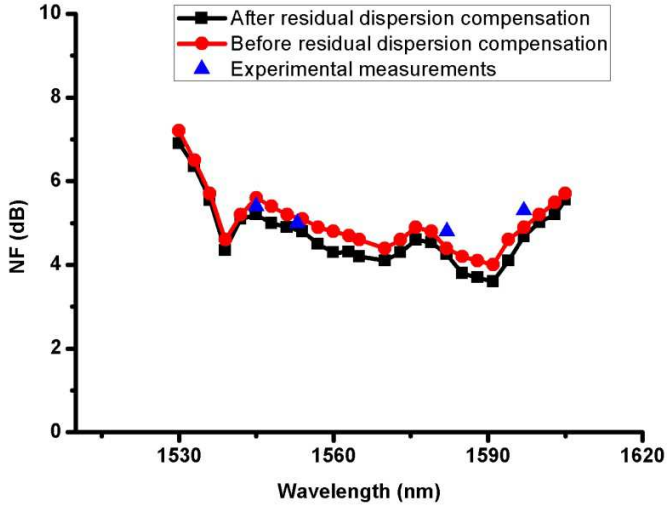

(c)

Fig. 4.7 (a): FBG reflectivity versus wavelength before and after gain equalization; (b): Gain versus wavelength of the hybrid fiber amplifier before and after equalization; (c): Simulated and measured noise figures versus wavelength of the fiber amplifier

In Fig. 4.7, we discuss the gain equalization issue. Using simulation software, the reflectivities of all the FBGs are set at 99% initially before gain equalization which is shown as black squares in Fig. 4.7 (a). Then we achieve gain equalization by adjusting FBGs' reflectivities with 99.9% for 1570 nm and 4.2% for 1605 nm channel individually as indicated by red circles. On the other hand, the experimentally measured FBGs reflectivities for 1545, 1553, 1582 and 1597 nm are 9.5%, 5.2%, 20.3% and 9.7%

respectively after gain equalization which is shown in Fig. 4.7 (a) by blue triangles. In Fig. 4.7 (b), simulation results show that the gain variation is as large as 4 dB among channels indicated by black squares before gain equalization. Nevertheless, the variation is greatly reduced to 0.5 dB after gain equalization by adjusting individual FBG's reflectivities which is shown by red circles in Fig. 4.7 (b). Experiment results also show the gain values for channels 1545, 1553, 1582 and 1597 nm are 4.6, 5.0, 4.8 and 5.1 dB (These values could be seen in Figures 4.8 (a) and (b)) respectively, which is shown as blue triangles. The simulation results are quite match to the experimental measurements. In this experiment a 60% reflectivity pump reflector was bought and used during measurement. The simulated NFs before and after residual dispersion compensation are shown as red circles and black squares, respectively in Fig. 4.7 (c). The measured NFs after residual dispersion compensation, using the polarization nulling method, for 1545-, 1553, 1582 and 1597 nm are 5.4, 5.0, 4.9 and 5.3 dB respectively, shown as blue triangles. In general, the L-band channels have lower NFs than the C-band channels. A double-path reflection design may degrade the NFs to some extent due to reflection and/or noise. The NF values ranged from 3.7 dB to 7.0 dB, which are still acceptable. We can see that the average NF is further reduced after residual dispersion compensation. In our design, the L band signals are amplified by RFA via DCF segments only. They did not transmit or interact with the EDF. Thus, the L band signals have no impact on the gain/power and NFs of the C-band signals. Vice versa, the C band signals neither affect the L band signals or NFs because the amount of residual pumping power to the C band EDF is fixed regardless what the

input C band signal levels are.

Hybrid fiber amplifier in WDM PON

Next, we apply the bidirectional hybrid amplifier in a 50-km WDM PON to investigate its ability to improve the performance of the network. And we take measurements from 4 channels to prove our concept. Fig. 4.8 (a) shows the experimentally measured C band signals at 1545 nm and 1553 nm before and after gain equalization, taken from a ratio coupler (RC1). In the other direction, Fig. 4.8 (b) shows the experimentally measured L band signals at 1582 and 1597 nm before and after gain equalization, taken from another ratio coupler (RC2), respectively. This proves our idea of suppressing gain variation through FBG reflectivity adjustment. Although the reduction in FBG reflectivity indeed degrades the signal-to-noise (SNR) somewhat, the SNR of 17-30 is still satisfied for 10Gb/s per channel digital transmission. Because each FBG sideband boundary is only 0.5 nm away from the FBG reflection spectrum center, it has no noise/dispersion effect on neighboring channels as the channel spacing is 3 nm for the simulation and even larger for the experiment.

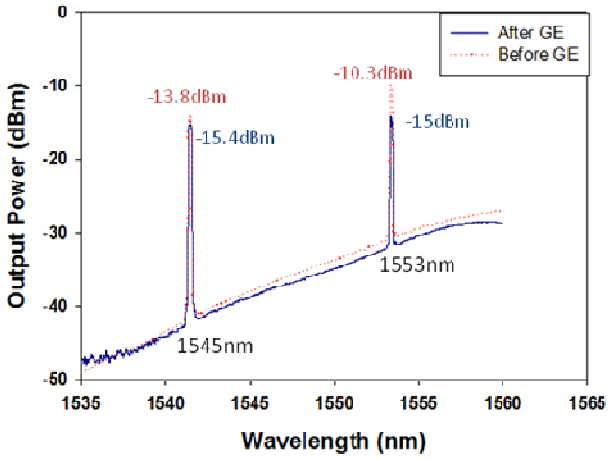

(a)

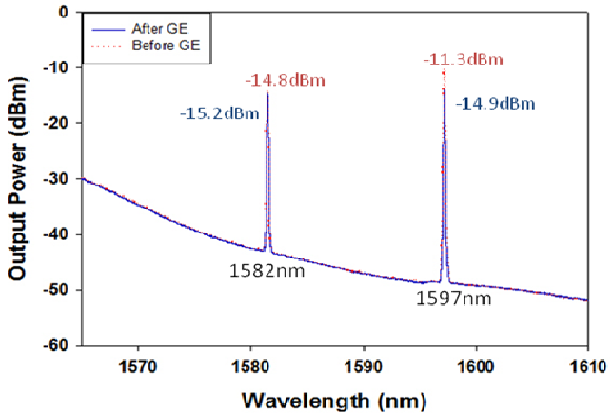

(b)

Fig. 4.8 (a): The measured C band wavelengths before and after gain equalization; (b): The measured L band wavelengths before and after gain equalization

The simulated Q values for the C+L band wavelengths are shown by red circles (before residual dispersion compensation) and black squares (after residual dispersion

compensation) in Fig. 4.9 (a). And the average Q values improved from 2.9 to 6.4 dB after appropriate dispersion compensation. Fig. 4.9 (b) shows the bit-error-rate (BER) against the received power, which is obtained from simulation (straight lines) and experimental measurement (dots) at 1553 nm for the C band and at 1582 nm for the L band, respectively. Both before and after residual dispersion compensation results are presented. In the simulation, first we use a common DCF segment for dispersion compensation, the BER at 10^{-9} is achieved -17.4 dBm for the 1553 nm channel and -17.6 dB m for 1582 nm received power, respectively. In this case, the chromatic dispersion is not compensated optimally for every channel. Then we precisely compensate the residual dispersion using our proposed dispersion compensation modules which consists of DCF segments and FBG arrays. And we can see the required signal power decreases by about 3 dB for both channels. The WDM PON performance improves obviously by using the proposed hybrid amplifier. The back-to-back transmission (simulated and experimentally measured) results for 1553 nm are also shown for comparison. We found that there is small power penalty between back-to-back and appropriate dispersion compensation. The power penalty may due to the extra fiber components, fiber splicing losses, amplifier NF and gain variation introduced. It is 1.5 dB on average, which is acceptable in transmission.

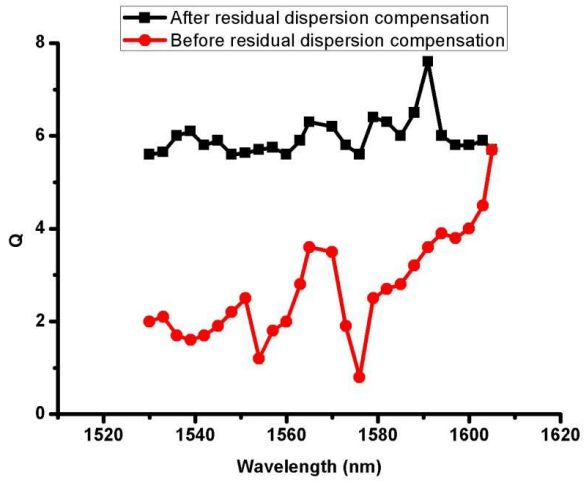

(a)

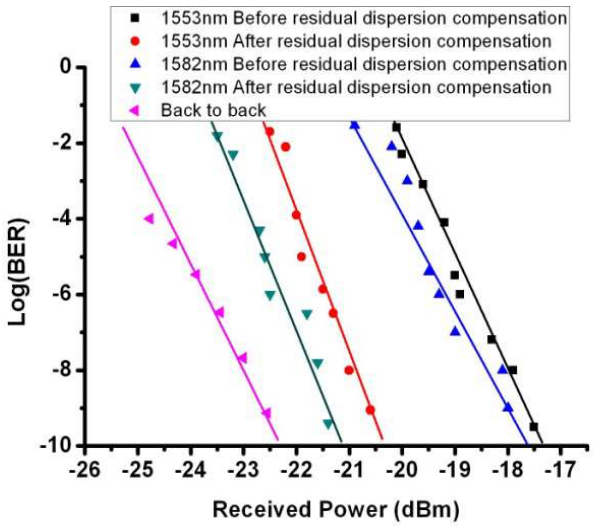

(b)

Fig. 4.9 (a): Simulated Q values before and after residual dispersion compensation; (b): Simulated and experimentally measured BER performances of the system before and after residual dispersion compensation

Eye diagrams are also provided for 1553 nm at BER of $2.0x10^{-10}$ before residual dispersion compensation in Fig. 4.10 (a) and at BER of $2.2x10^{-11}$after residual dispersion compensation in Fig. 4.10 (b). The measurements in eye S/N and ext. ratio show improvement after residual dispersion compensation but it is not significant. The reason why the improvement is not obvious is that both BER are small and acceptable ($<1.0x10^{-9}$), so the differences in eye diagrams are not very significant in that case. To prove that, simulation has been done and the simulated eye diagrams for BER of $2.0x10^{-10}$ and BER of $2.2x10^{-11}$ are shown in Fig. 4.11 (a) and (b) respectively.

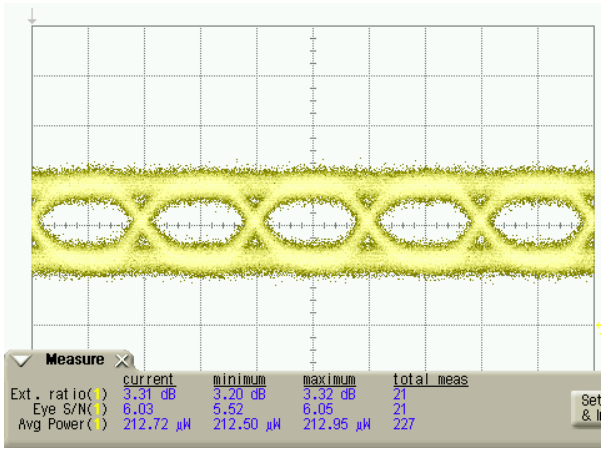

(a)

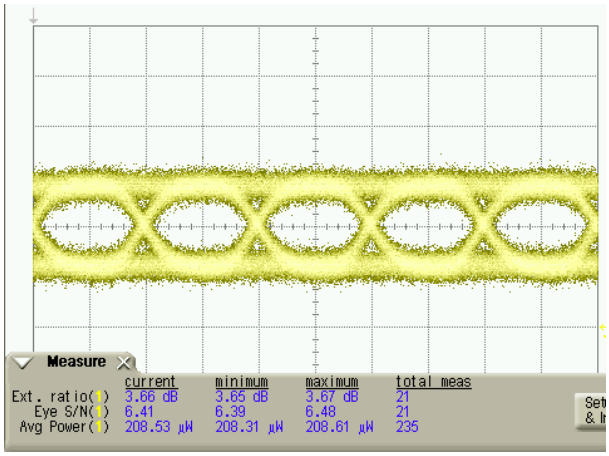

(b)

Fig. 4.10(a): Eye diagram for 1553 nm at 2.0 x10^{-10} before residual dispersion compensation; (b): Eye diagram for 1553 nm at 2.2 x10^{-11} after residual dispersion compensation

And we can see from Fig. 4.11 that differences between eye diagrams at BER of 2.0x10^{-10} and BER of 2.2x10^{-11} are not obvious either.

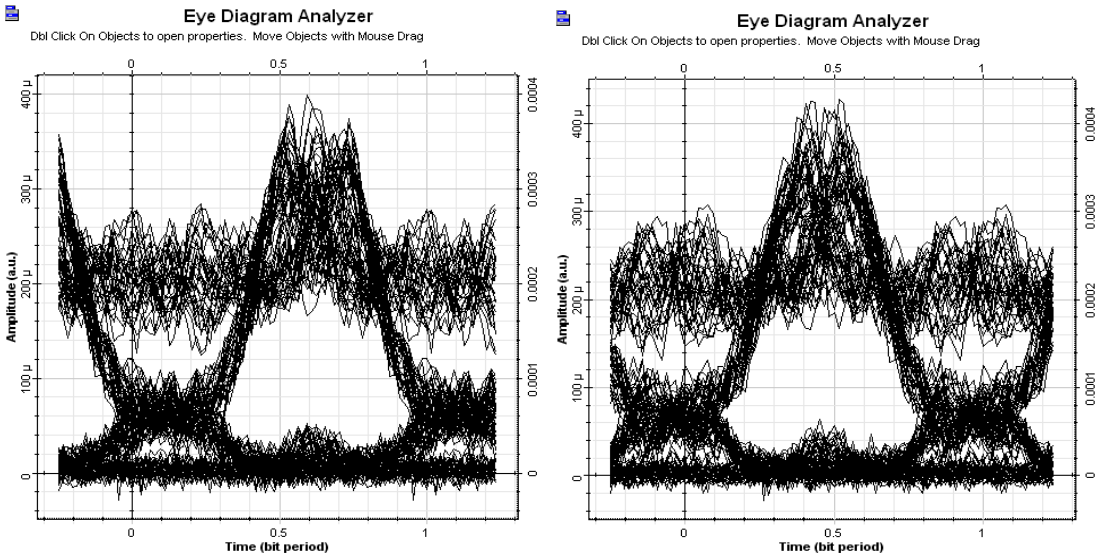

(a) (b)

Fig. 4.11: Simulation results for eye diagrams at (a) BER of 2.0 x10^{-10}; (b)BER of 2.2 x10^{-11}

Although we proposed a C+L band EDFA/RFA using a single-pump at 1480 nm [78], the gain profile drops when the signal wavelength exceeds 1595 nm (the longer wavelength region of L band) due to boundary the Raman shift gain region. The proposed hybrid fiber amplifier with single wavelength pump LD at 1495 nm, although downgrades the gain of C band a little, it can extend the Raman gain profile up to 1610 nm easily.

4.4 Conclusions

In this chapter, we introduce two configurations of hybrid pump which can cover C+L band using a single pumping LD. First a unidirectional hybrid C+L band EDFA/RFA has been proposed utilizing a 1480 nm pumping LD. It has a loop-back scheme bridged by the double-passed dispersion compensator for both the C+L band channels. Power equalization for the 14 WDM channels is realized by adjusting the pump ratio and optimizing the FBG reflectivity for the corresponding channels. At an input power of -20 dBm/ch, power variations among all channels are reduced from 6.5 dB to less than ±0.2 dB after gain equalization. To increase the pump efficiency, both the signals and pumping power double-pass the gain medium. A single pump reflector is shared by both the C and L bands to recycle the residual pumping power. This kind of hybrid EDFA/RFA may find vast applications in WDM long-haul systems and optical networks where dispersion management, power budget and power equalization are crucial issues.

Then, we improve the previous configuration thus proposed a bidirectional hybrid C+L band EDFA/RFA scheme for WDM PONs amplification. The hybrid amplifier could work full duplex bi-directionally. Single wavelength pump LD at 1595 nm was used and its pumping efficiency improved by recycling the residual pumping power. Using the FBG arrays together with the DCF, chromatic dispersion for all channels could be optimally compensated. Compared with conventional dispersion compensation using a common

DCF section for all channels, the proposed hybrid fiber amplifier improved the system Q value from 2.9 to 6.4 among 26 C+L channels at 10 GB/s per channel. The required average received power for error free transmission was reduced by 3dB. The gain fluctuation could be reduced from 4 dB to less than 0.5 dB by adjusting the FBG reflectivity. Four channels for 50-km WDM PON transmission using this hybrid amplifier were experimentally analyzed without loss of generality. Both the bi-directional hybrid fiber amplifier and system performance characteristics in 50-km WDM PON were measured to confirm the feasibility of this hybrid fiber amplifier. With these advantages, this hybrid fiber amplifier is able to find vast applications in bi-directional WDM PON systems where both dispersion management and gain equalization are crucial issues.

Chapter 5 Conclusions and Recommendations for Future works

5.1 Conclusions

This thesis has presented the applications of optical amplifier in next generation optical communication networks. In order to better understand the gain characteristics of SOA, we have performed both simulation and experiments to find the discrepancy between the existing formula and the experimental results. Then we carried out theoretical investigations to find out that the internal loss inside the SOA active region, which cannot be ignored under high injection power, is the cause of discrepancy. Next we proposed a new formula containing the internal loss factor. And we experimentally verify the accuracy of the new proposed formula. In addition, we tested another SOA from a different company and thus prove the feasibility of this formula to different kinds of SOA.

We have proposed a novel configuration of all-optical switch utilizing the NPR in SOA. A linear polarization state was maintained during the process of NPR. The complete switching of light from one output port to another was experimentally first. Then a data packet containing 500 bytes PRBS data at bit rate of 2.5 Gb/s was introduced to the switch.

It was switched successfully from one output port to another with an extinction ratio of 20 dB. The average control power injected was 0 dBm and the eye diagrams showed the signal details were maintained well. Next, we introduced a novel configuration of fiber loop type all-optical buffer based on the all-optical switch proposed together with PMF. The buffering results of 2.5 Gb/s data packet mixed with RF signal from 10 GHz to 40 GHz have been theoretically studied. Effects of input signal power, control signal power, SOA biasing current and control signal polarization were investigated and thus optimized. In addition, a negative format of control signal was proposed to reduce the effect of cross gain polarization in SOA. And we achieved storage of 1.2 μs for microwave signal at 10 GHz. In case the frequency of microwave signal increases to 40 GHz, the maximum acceptable storage time we obtained is 600 ns.

We have proposed a hybrid pump covering C+L band. We introduced a novel configuration of unidirectional hybrid pump which employs EDFA for C band and RFA for L band amplification. Residual pump reuse was utilized to improve the efficiency. Thus EDFA and RFA shared one pumping LD at 1480 nm. An array of FBGs together with DCF was introduced to suppress the gain variation and accurately compensate the chromatics dispersion. Gain variation has been reduced from 6.5 to 0.2 dB and the noise distribution analysis indicated the capability of amplification with negligible intra-band cross talk. Then we modified the schematic further to make it a bidirectional pump for application in WDM PON. The pumping LD wavelength was shifted to 1495 nm to cover the whole L band. Then we tested it in a 50 km WDM PON with 26 channels at data rate

of 10 Gb/s/channel. With the help of accurate chromatic dispersion compensation, the system Q value was increased from 2.9 to 6.4 at -20 dBm input power. Investigations also indicated that the average required received power to achieve error free transmission (BER<10^{-9}) was reduced by 3 dB. Moreover, the gain variation has been suppressed from as large as 4 dB to less than 0.5 dB successfully. Four channels for 50-km WDM PON transmission using this hybrid amplifier were experimentally analyzed without loss of generality. Both the bi-directional hybrid fiber amplifier and system performance characteristics in 50-km WDM PON were measured to confirm the feasibility of this hybrid fiber amplifier.

5.2 Recommendation for future works

Although an intensive investigation of applications of optical amplifiers in optical communication networks has been conducted in this thesis, with the rapid technological developments, there still exits some interesting research possibilities that are worth doing for future works.

5.2.1 all-optical logic gates based on nonlinearity in SOA

Recently, great attention has been paid to all-optical signal processing based on nonlinearities in SOA. Special attention has been paid to all-optical logic gates using SOA as they are crucial components for all-optical signal processing. Among all the technology reported, SOA attracts considerable attention because of its compact size, low power consumption and ease of integration with other devices. Several techniques have been reported to realize all-optical logic gates using SOA. In [79], a 20 Gb/s all-optical OR logic gate for returnto- zero-on-off-keying (RZ-OOK) signals has been presented using nonlinear polarization rotation (NPR) in the SOA. Another logic gate based employing cross-gain modulation (XGM) and four-wave mixing (FWM) in SOA has been demonstrated [80]. Wu et al. demonstrated another schematic of simultaneous OR and AND gate for RZ/CSRZ/NRC OOK utilizing FWM in SOA. Recently, differential phase shift keying (DPSK) signal format has drawn a lot of attention because of its low channel power and long transmission distance compared with OOK format [81]. Several works on DPSK logic gates has been reported [82-83]. However, there is no report on all-optical NOT gate based on FWM in SOA.

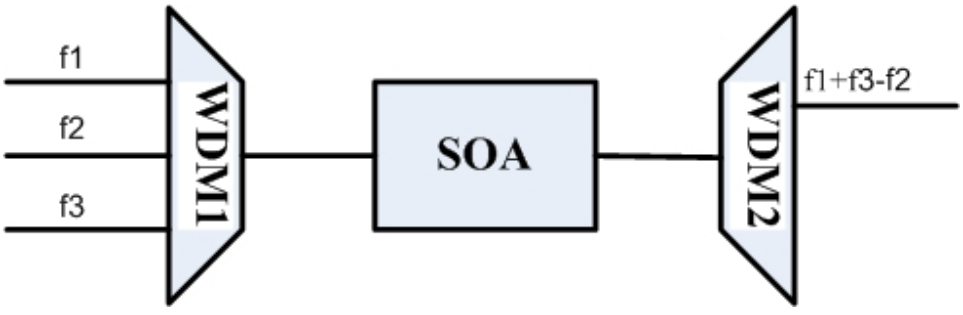

Fig. 5.1: Proposed schematic for all-optical NOT gate

As shown in Fig. 5.1, three FWM participators are injected into the SOA. f1 carries the RZ-DPSK data while f2 is a continuous wave pump light. f3 is a CSRZ-clock introduced. After coming out from SOA, there are a few new wavelength components. And they have a frequency which can be predicted by the following equation:

$$f_{lmn} = f_l + f_m - f_n \tag{5.1}$$

where l, m, n stand for the three input wavelengths. The output phases also have the same relationship.

$$\phi_{lmn} = \phi_l + \phi_m - \phi_n \tag{5.2}$$

We select the components which has a frequency of f1+f3-f2 as the output for NOT gate. And the following table illustrate the idea of all-optical NOT gate utilizing FWM in SOA, where phase of f2 is 0.

Table 5.1: Logic table for all-optical NOT gate

Data f1	1	1	0	0	1	0	1	0	1	1	1	0	0	0	1
RZ-DPSK	0	π	π	π	0	0	π	π	0	π	0	0	0	0	π
CSRZ clock f3	0	π	0	π	0	π	0	π	0	π	0	π	0	π	0
f1+ f3- f2	0	0	π	0	0	π	π	0	0	0	0	π	0	π	Π

NOT Data	0	0	1	1	0	1	0	1	0	0	0	1	1	1	0
RZ-DPSK	0	0	π	0	0	π	π	0	0	0	0	π	0	π	π

5.2.2 Cascadability of proposed all optical buffer and dual-wavelength packet buffering

For the proposed schematic of fiber loop type all-optical buffer utilizing NPR in SOA, we are also interested in the cascadability of this scheme. Two or more all-optical buffer will be cascaded to investigate the buffering results. Amplified spontaneous emission (ASE) noise will be accumulated during each stage and thus affect the next stage of buffer. The impact of accumulating ASE noise will be analyzed and parameters will be optimized to suppress the ASE noise. Chromatic dispersion is also a problem in case there are a number of buffers cascaded together where long buffering time is required. Investigation will also be carried out to observe the chromatic dispersion behavior and solutions will be proposed to reduce the effect of chromatic dispersion.

The ability of the buffer to handle more than one wavelength data packets will be investigated. Two data packets with different wavelengths overlapping in time domain will affect the polarization state of each other. Consequently, the buffering results will not be as good as before. However, carefully adjusting the ratio of control power to input signal power will reduce the polarization state difference between the two data packets.

Conclusions and Recommendations for Future works

Analysis will be done to find the working conditions which give the best buffering results for both data packets.

References

[1] K. C. KAO and G. HOCKHAM, "Dielectric fiber surface waveguide for optical frequencies," IEE Proc., 113, 1151-1158, 1966.

[2] F. P. Kapron, D. B. Keck, and R. D. Maurer, “Radiation losses in glass optical waveguides,” IEE Conf. Trunk Telecommunications by Guided Waves, **71**, 148-153, 1970.

[3] W. L. Ha, R. M. Fortenberry, and R. S. Tucker, "Demonstration of photonic fast packet switching at 700 Mbit/s data rate," Electron. Lett., **27**, 789-790, 1991.

[4] T. Otani, “All-optical networking testbed demonstration,” International Conference on Photonics in Switching, 154-155, 2008.

[5] J. D. Downie, J. Hurley, S. Ten, C. Towery, M. Sharma, Y. Mauro, C. Malouin, B. Zhang, J. Bennike, T. Schmidt, and R. Saunders, "DWDM 43 Gbit/s DPSK transmission over 1200 km with no inline dispersion compensation," Electron. Lett., **46**, 60-61, 2010.

[6] Y. Miyamoto, K. Yonenaga, A. Hirano, H. Toba, K. Murata, and H. Miyazawa, "100 GHz-spaced 8 x 43 Gbit/s DWDM unrepeatered

References

transmission over 163 km using duobinary-carrier-suppressed return-to-zero format," Electron. Lett., **37**, 1395-1396, 2001.

[7] R. J. Mears, L. Reekie, I. M. Jauncey, and D. N. Payne, "Low-noise Erbium-doped fiber amplifier operating at 1.54-mu-m," Electron. Lett., **23**, 1026-1028, 1987.

[8] E. Desurvire, J. R. Simpson, and P. C. Becker, "HIGH-GAIN ERBIUM-DOPED TRAVELING-WAVE FIBER AMPLIFIER," Optics Lett., **12**, 888-890, 1987.

[9] G. Zeidler and Schicket.D, "USE OF LASER AMPLIFIERS IN A GLASS-FIBER COMMUNICATIONS SYSTEM," Radio and Electronic Engineer, **43**, 675-682, 1973.

[10] Personic.Sd, "APPLICATIONS FOR QUANTUM AMPLIFIERS IN SIMPLE DIGITAL OPTICAL COMMUNICATION SYSTEMS," Bell System Technical Journal, **52**, 117-133, 1973.

[11] Y. Yamamoto, "CHARACTERISTICS OF ALGAAS FABRY-PEROT CAVITY TYPE LASER-AMPLIFIERS," IEEE J. Quantum Electron., **16**, 1047-1052, 1980.

[12] T. Mukai, Y. Yamamoto, and T. Kimura, "S/N AND ERROR RATE PERFORMANCE IN ALGAAS SEMICONDUCTOR-LASER PRE-AMPLIFIER AND LINEAR REPEATER SYSTEMS," IEEE J. Quantum Electron., **18**, 1560-1568, 1982.

References

[13] J. C. Simon, "GAINASP SEMICONDUCTOR-LASER AMPLIFIERS FOR SINGLE-MODE FIBER COMMUNICATIONS," IEEE J. Lightwave. Tech., **5**, 1286-1295, 1987.

[14] C. E. Zah, C. Caneau, F. K. Shokoohi, S. G. Menocal, F. Favire, L. A. Reith, and T. P. Lee, "1.3MU-M GAINASP NEAR-TRAVELING-WAVE LASER-AMPLIFIERS MADE BY COMBINATION OF ANGLED FACETS AND ANTIREFLECTION COATINGS," Electron. Lett., **24**, 1275-1276, 1988.

[15] N. A. Olsson, R. F. Kazarinov, W. A. Nordland, C. H. Henry, M. G. Oberg, H. G. White, P. A. Garbinski, and A. Savage, "POLARIZATION-INDEPENDENT OPTICAL AMPLIFIER WITH BURIED FACETS," Electron. Lett., **25**, 1048-1049, 1989.

[16] G. P. Agrawal, Nonlinear Fiber Optics, 2nd ed., Academic, New York, 1995.

[17] R. H. Stolen, and E. P. Ippen, “Raman gain in glass optical waveguides,” Appl. Phys. Lett., **22**, 276-278, 1973.

[18] Y. Aoki, S. Kishida, K. Washio, and K. Minemura, “Bit error rate evaluation of optical signals amplified via stimulated Raman process in an optical fiber,” Electron. Lett., **21**, 191-193, 1985.

References

[19] L. F. Mollenauer, J. P. Gordan, and M. N. Islam, “Soliton propagation in long fibers with periodically compensated loss,” IEEE J. Quantum Electron., **22**, 157- 173, 1986.

[20] R. Langenhorst, M. Eiselt, W. Pieper, G. GroBkopf, R. Ludwig, L. Kuller, E. Dietrich, and H. G. Weber, "Fiber Loop Optical Buffer," IEEE J. Lightwave. Tech., **14,** 324-335, 1996.

[21] X. Hong, Y. Chen and J. Lin, "Erasable Fiber Loop Optical Buffer," Fifth Asia-Pacific Conference on Communications and Fourth Optoelectronics and Communications Conference, 1406, 1999.

[22] A.M. Liu, C.Q. Wu, M.S. Lim, Y.D. Gong and P. Shum, "Dual-Loop Optical Buffer (DLOB) Based on a 3 by 3 Collinear Fiber Coupler," IEEE Photo. Tech. Lett., **16**, 2129-2131, 2004.

[23] S. Fu, P. Shum, L. Zhang, C. Wu, and A. M. Liu, " Design of SOA-Based Dual-Loop Optical Buffer With a 3 × 3 Collinear Coupler: Guideline and Optimizations," IEEE J. Lightwave. Tech., **24**, 2768-2778, 2006.

[24] C. Chen, L. A. Johansson, V. Lal, M. L. MaSanoviC, D. J. Blumentbal and L. A. Coldren, "Programmable Optical Buffering using Fiber Bragg Gratings combined with a Widely-Tunable Wavelength Converter," Optical Fiber Communication Conference, **3**, 3, 2005.

References

[25] M. P. Fok and C. Shu, "Tunable optical delay using four-wave mixing in a 35-cm highly nonlinear bismuth-oxide fiber and group velocity dispersion," IEEE J. Lightwave. Tech., **26**, 499-504, 2008.

[26] H. Park, J. P. Mack, D. J. Blumenthal, and J. E. Bowers, "An integrated recirculating optical buffer," Optics Express, **16**, 11124-11131, 2008.

[27] G. Berrettini, G. Meloni, L. Poti, and A. Bogoni, "All-Optical Variable Buffer Based on Semiconductor Optical Amplifier," IEEE J. Quantum Electron., **47**, 510-516, 2011.

[28] J. B. Khurgin, "Light slowing down in Moire´ fiber gratings and its implications for nonlinear optics," Phy. Rev. A, **62**, 013821, 2000.

[29] G. Lenz, B. J. Eggleton, C. K. Madsen, and R. E. Slusher, " Optical Delay Lines Based on Optical Filters," IEEE J. Quantum Electron., **37**, 525-532, 2001.

[30] J. E. Sharping, Y. Okawachi, and A. L. Gaeta, “Wide bandwidth slow light using a Raman fiber amplifier," Optics Express, **13**, 6092-6098, 2005.

[31] Z. Chen, B. Pesala and C. Hasnain, "Experimental Demonstration of Slow Light via Four-Wave Mixing in Semiconductor Optical Amplifiers," Optical Fiber Communication Conference, **1-6**, 1032-1034, 2006.

[32] D. Mori and T. Baba, "Wideband and low dispersion slow light by chirped photonic crystal coupled waveguide," Optics Express, **13**, 9398-9408, 2005.

References

[33] P. Horak, W. Stewart, and W. H. Loh, "Continuously tunable optical buffer with a dual silicon waveguide design," Optics Express, **19**, 12456-12461, 2011.

[34] J. J. Yu, X. Zhou, and M. F. Huang, "High-Speed PDM-RZ-8QAM DWDM Transmission (160 x 114 Gb/s) Over 640 km of Standard Single-Mode Fiber," IEEE Photon. Technol. Lett., **21**, 1299-1301, 2009.

[35] A. R. Moral, P. Bonenfant, S. Baroni, R. Wu, "Optical data networking: protocols, technologies, and architectures for next generation optical transport networks and optical internetworks," IEEE J. Lightwave Technol., **18**, 1855-1870, 2000.

[36] J.R. Stern, C.E. Hoppitt, D.B. Payne, M.H. Reeve, and K. Oakley, "TPON-a passive optical network for telephony," Optical Communication, 1988. (ECOC 88), **1**, 203-206 1988.

[37] ITU-T Recommendation G.984.1: "General characteristics for Gigabitcapable Passive Optical Networks".

[38] X. Zhou, C. Lu, P. Shum, and T. H. Cheng, "A simplified model and optimal design of a multiwavelength backward-pumped Raman amplifier," IEEE Photon. Technol. Lett., **13**, 945–947, 2001.

[39] Carena, V. Curri, and P. Poggiolini, "On the optimization of hybrid Raman/Erbium-doped fiber amplifiers," IEEE Photon. Technol. Lett., **13**, 1170-1172, 2001.

References

[40] S. Park , G. Kim and T. Park, “WDM-PON system based on the laser light injected reflective semiconductor optical amplifier,” Optical Fiber Technology, **12**, 162–169, 2006.

[41] T. B. Gibbon, K. Prince, T. T. Pham, A. Tatarczak, C. Neumeyr, E. Ronneberg, M. Ortsiefer, and I. T. Monroy, "VCSEL transmission at 10 Gb/s for 20 km single mode fiber WDM-PON without dispersion compensation or injection locking," Optical Fiber Technology, **17**, 41-45, 2011.

[42] K. Y. Cho, Y. Takushima, and Y. C. Chung, "10-Gb/s Operation of RSOA for WDM PON, " IEEE Photon Technol Lett., **20**, 1533-1535, 2008

[43] P. Healey, P. Townsend, C. Ford, L. Johnston, P. Townley, I. Lealman, L. Rivers, S. Perrin and R. MooreSpectral, "Slicing WDM-PON using wavelength-seeded reflective SOAs," Electron. Lett., **37**, 1181-1182, 2001.

[44] H. Masuda, S. Kawai, “Wide-band and gain-flattened hybrid fiber wide-band and gain-flattened hybrid fiber,” IEEE Photon. Technol. Lett., **11**, 647-649, 2002.

[45] Y. Emori, S. Matsushita and S. Namiki, “Cost-effective depolarized diode pump unit designed for C-band flat-gain Raman amplifiers to control EDFA gain profile,” Proc. Optical Fiber Communication Conference, 106-108, 2000.

References

[46] H. Lee, Y. M. Chang, Y. G. Han, S. H. Kim, H. Y. Chung, and S. B. Lee, "Dispersion-compensating Raman/EDFA hybrid amplifier recycling residual Raman pump for efficiency enhancement," IEEE Photon. Technol. Lett., **17**, 43-45, 2005.

[47] J. W. Nicholson, "Dispersion compensating Raman amplifiers with pump reflectors for increased efficiency," J. Lightw. Technol., **21**, 1758–1762, 2003.

[48] H. S. Seo, Y. G. Choi, B. J. Park, D. H. Cho, and K. H. Kim, "Simultaneous amplification by Er ions and SRS in an Er-doped Germano-Silica fiber," IEEE Photon. Technol. Lett., **15**, 1198-1200, 2003.

[49] H. S. Seo, J. T. Ahn, B. J. Park and W. J. Chung, "Double pass Er-Raman amplifier," Electron. Lett., **13**, 801-802, 2007.

[50] S. K. Liaw, C. K. Huang, and Y. L. Hsiao, "Parallel-type C+L band hybrid amplifier pumped by 1480 nm laser diodes," Laser Phys. Lett., **5**, 543-546, 2008.

[51] S. K. Liaw and Y. S. Huang, "C+L-band hybrid amplifier using FBGs for dispersion compensation and power equalisation," Electron. Lett., **44**, 844-U166, 2008.

[52] S. K. Liaw, L. Dou, and A. Xu, "Fiber-Bragg-grating-based dispersion-compensated and gain-flattened raman fiber amplifier," Optics Express, **15**, 12356-12361, 2007.

References

[53] T. Houbavlis, K. E, Zoiros, M. Kalyvas, G. Theophilopoulos, C. Bintjas, K. Yiannopoulos, N. Pleros, K.Vlachos, H. Avramopoulos, L. Schares, L. Occhi, G. Guekos, J. R. Taylor, S. Hansmann, and W. Miller. "All-optical signal Processing and applications within the esprit project DO-ALL," IEEE J. Lightwave. Technl., **23**, 781-801, 2005.

[54] V. V. Lysak, H. Kawaguchi, and I. A. Sukhoivanov. "Gain spectra and saturation power of asymmetrical multiple quantum well semiconductor optical amplifiers," IEE Proceedings of Optoelectronics, **152**,131-139, 2005.

[55] D. Cotter, R. J. Manning, K. J. Blow, A. D. Ellis, A. E. Kelly, D. Nesset, I. D. Phillips, A. J. Poustie, and D. C. Rogers. "Non-linear Optics for High-Speed Digital Information Processing," Science, **286**, 1523-1528, 1999.

[56] A. Bogoni, L. Poti, C.Porzi, M. Scaffardi, P. Ghelfi, and F. Ponzini. "Modeling and measurement of noisy SOA dynamics for ultrafast applications," IEEE J. Sel. Quantum Electron., **10**, 197-205, 2004.

[57] J. Bibong, J. W. Goodman. "Gain optimization in switches based on semiconductor optical amplifiers," IEEE J. Lightwave. Technl., **13**, 598-605, 1995.

[58] H. Ghafouri-Shiraz, "Fundamentals of laser Diode Amplifiers," John Wiley, 1995.

References

[59] N. K. Dutta, and Q. Wang, “Semiconductor Optical Amplifiers,” World Scientific, 2006.

[60] Y. Yamamoto, “Characteristics of AlGaAs Fabry-Perot cavity type laser amplifiers,” IEEE J. Quantum Electron., **16**, 1047-1052, 1980.

[61] T. Mukai, Y. Yamamoto and T. Kimura, “S/N and error rate performance in AlGaAs semiconductor laser preamplifier and linear repeater systems,” IEEE Trans. Microwave Theory and Tech., **30**, 1548-1552, 1982.

[62] J. C. Simon, “GalnAsP semiconductor laser amplifiers for single mode fibre communications,” IEEE J. Lightwave Technol., **5**, 1286-1295, 1987.

[63] C. Joergensen, S. L. Danielsen, K. E. Stubkjaer, M. Schilling, K. Daub, P. Doussiere, F. Pommerau, P. B. Hansen, H. N. Poulsen, A. Kloch, M. Vaa, B. Mikkelsen, E. Lach, G. Laube, W. Idler, and K. Wunstel, "All-optical wavelength conversion at bit rates above 10 Gb/s using semiconductor optical amplifiers," IEEE J. Sel. Quantum Electron., **3**, 1168-1180, 1997.

[64] O. Kamatani and S. Kawanishi, "Ultrahigh-speed clock recovery with phase lock loop based on four-wave mixing in a traveling-wave laser diode amplifier," IEEE J. Lightwave Technol., **14**, 1757-1767, 1996.

[65] Q. Wang, F. Zeng, S. Blais, and J. P. Yao, "Optical ultrawideband monocycle pulse generation based on cross-gain modulation in a semiconductor optical amplifier,"Optics Lett., **31**, 3083-3085, 2006.

References

[66] C. Y. J. Chu, H. Ghafouri-Shiraz. "Analysis of gain and saturation characteristics of a semiconductor laser optical amplifier using transfer matrices," IEEE J. Lightwave. Technl., 12, 1378-1386, 1994.

[67] A. A. M. Saleh. "Nonlinear models of travelling-wave optical amplifiers," Electron. Lett., **24**, 835-837, 1988.

[68] W. W. Chow and R. R. Craig, "Amplified spontaneous emission effects in semiconductor laser amplifiers," IEEE J. Quantum Electron., **26**, 1363-1368, 1990.

[69] A. Reale, A. D. Carlo, and P. Lugli, "Gain dynamics in traveling-wave semiconductor optical amplifiers," IEEE J. Sel. Quantum Electron., **7**, 293-299, 2001.

[70] Y.Ben-Ezra, M.Haridim, and B. I. Lembrikov, "Theoretical analysis of gain-recovery time and chirp in QD-SOA," IEEE Photon. Technol. Lett., **17**, 1803-1805, 2005.

[71] C.M. Gallep, R. P. Vivacqua, A.L.R. Cavalcanti, and E. Conforti, "Calibration of semiconductor optical amplifier simulator for switching action prediction," Proc. 2003 SBMO/IEEE MTT-S International, **1**, 129-132, 2003.

[72] Connelly, M. J. "Wide-Band Steady-State Numerical Model and Parameter Extraction of a Tensile-Strained Bulk Semiconductor Optical Amplifier," IEEE J. Quantum Electron., **43**, 47-56, 2007.

References

[73] G. P. Agrawal and N. A. Olsson. “Self-phase modulation and spectral broadening of optical pulses in semiconductor laser amplifiers,” IEEE J. Quantum Electron**., 5**, 2297-2306, 1989.

[74] S. Fu, W. D. Zhong, P. Shum, C. Q. Wu, and J. Q. Zhou, "Nonlinear polarization rotation in semiconductor optical amplifiers with linear polarization maintenance," IEEE Photon. Technol. Lett., **19**, 1931-1933, 2007.

[75] M. Wegert, N. Majer, K. Ludge, S. Dommers-Volkel, J. Gomis-Bresco, A. Knorr, U. Woggon, and E. Scholl, "Nonlinear gain dynamics of quantum dot optical amplifiers," Semiconductor Science and Technology, **26**,014008, 2011.

[76] C. S. Cleary, M. J. Power, S. Schneider, R. P. Webb, and R. J. Manning, "Fast gain recovery rates with strong wavelength dependence in a non-linear SOA," Optics Express, **18**, 25726-25737, 2010.

[77] L Kazovsky, S. Benedetto and A. Willner, Optical fiber Communication Systems, 1st ed., Artech House Publishers, Norwood, 1996.

[78] S. K. Liaw, Y. S. Huang, N. K. Chen and K. C. Hsu, “Dispersion management and gain flattened a hybrid EDFA/RFA in pumping recycling mechanism,” IEEE Conference on Lasers and Electro-Optics, **1**, 999-1000, 2008.

References

[79] J. Zhang, J. Wu, C. Feng, K. Xu, and J. Lin, "All-Optical Logic Gate Exploiting Nonlinear Polarization Rotation in an SOA and Red-Shifted Sideband Filtering," IEEE Photon. Technol. Lett., **19**, 33-35, 2007.

[80] G. Berrettini, A. Simi, A. Malacarne, A. Bogoni, and L. Poti, "Ultrafast integrable and reconfigurable XNOR, AND, NOR, and NOT photonic logic gate," IEEE Photon. Technol. Lett., **18**, 917-919, 2006.

[81] J. X. Cai, M. Nissov, D. G. Foursa, C. R. Davidson, L. Liu, Y. Cai, A. N. Pilipetskii, W. W. Patterson, G. Domagala, H. Li, and N. S. Bergano, "Experimental comparison of DPSK and OOK modulation formats over slope- matched fiber spans," Optical Fiber Communication Conference, **2**, 3-5, 2004.

[82] C. Kit, C. Chun-Kit, C. Lian Kuan, and F. Tong, "Demonstration of 20-Gb/s all-optical XOR gate by four-wave mixing in semiconductor optical amplifier with RZ-DPSK modulated inputs," IEEE Photon. Technol. Lett., **16**, 897-899, 2004.

[83] N. Deng, K. Chan, C. K. Chan, and L. K. Chen, "An all-optical, XOR logic gate for high-speed RZ-DPSK signals by FWM in semiconductor optical amplifier," IEEE J. Sel. Quantum Electron., **12**, 702-707, 2006.

Author's Publications

Journal papers:

[1] Guo N., Fu S., Shum P., Wu C., Lim D. R., "Effect of absorption loss on the saturation characteristics of semiconductor optical amplifier", Optical Engineering, Vol 47, 3, 035004, 2008.
[2] Guo N., Fu S., Shum P., Wu C., "All optical buffer based on nonlinear polarization rotation (NPR) in semiconductor optical amplifier (SOA) for storage of microwave signal up to 40 GHz," Optics Communications (submitted)
[3] Guo N., Liaw S., Shum P., Chen N., Hung H., Lin C., "Single-Wavelength-Pump-Based Bidirectional Hybrid Fiber Amplifier for Bidirectional Local Area Network Application," Optics Communications (Accepted)
[4] Fu S., Shum P., Guo N., Wu C., Li Y., "Theoretical investigation of dual-wavelength packet signal storage with SOA-based dual loop optical buffer", Optics Communications, 279, 255, 2007.
[5] Tian C., Wu C., Li Z., Guo N., "Dual-Wavelength Packets Buffering in Dual-Loop Optical Buffer", Photonics Technology Letters, Vol 20, 8, 578, 2008.
[6] Liaw s., Huang Y., Guo N.,Shin C., Chen N., Hsu K., Dong J., Shum P., "Bridge-Scheme C+L Band Hybrid Amplifier with Optimum Dispersion Compensation and Gain Equalization," Microwave and Optical Technology Letters (submitted)

Conference papers:

[1] Guo N., Shum P., Wu C., Lim D. R., Wong V., "All-optical switch based on nonlinear polarization rotation (NPR) in semiconductor optical amplifier (SOA)", Asia-Pacific Optical Communications (APOC)2008
[2] Guo N., Liaw S., Shum P., Chen N., Lin C., "Bidirectional C+L Band Hybrid Amplifier for 16-Channel WDM PON Transmission at 10Gb/s," OptoElectronics and Communications Conference (OECC) 2010
[3] Shum P., Fu S., Guo N, Wu C. Li Y., "Design and Implementation of Optical Buffer with Networking Applications," Asia-Pacific Optical Communications (APOC)2008, (Invited talk)